LDL-mimetic lipid nanoparticles prepared by surface KAT ligation for *in vivo* MRI of atherosclerosis

Alessandro Fracassi,[a] Jianbo Cao,[b] Naoko Yoshizawa-Sugata,[c] ÉvaTóth,[d] Corey Archer,[e] Olivier Gröninger,[f] Emanuela Ricciotti,[g] Soon Yew Tang,[g] Stephan Handschin,[h] Jean-Pascal Bourgeois,[i] Ankita Ray,[a] Korinne Liosi,[a] Sean Oriana,[a] Wendelin Stark,[h] Hisao Masai,[c] Rong Zhou,*[b] and Yoko Yamakoshi*[a]

[a]Laboratorium für Organische Chemie, ETH Zürich, Vladimir-Prelog-Weg 3, CH-8093 Zürich, Switzerland, [b]Department of Radiology, University of Pennsylvania, Institute for Translational Medicine and Therapeutics, John Morgan 198, 3620 Hamilton Walk, Philadelphia, PA19104, USA, [c]Department of Genome Medicine, Tokyo Metropolitan Institute of Medical Science, 2-1-6 Kamikitazawa, Setagaya, Tokyo 156-8506, Japan, [d]Centre de Biophysique Moléculaire, CNRS UPR 4301, University of Orléans, Rue Charles Sadron, 45071 Orléans, Cedex 2, France, [e]Institut für Geochemie und Petrologie, ETH Zürich, Clausiusstrasse 25, CH-8092 Zürich, Switzerland, [f]Institute for Chemical and Bioengineering, ETH Zurich, Vladimir-Prelog-Weg 1, CH-8093 Zurich, Switzerland, [g]Department of Systems Pharmacology and Translational Therapeutics, University of Pennsylvania, Philadelphia, PA, USA, [h]Scientific Center for Optical and Electron Microscopy, ETH Zürich, Auguste-Piccard-Hof 1, CH-8093, Zürich, Switzerland, [i]University of Applied Science and Arts Western Switzerland, Bd de Pérolles 80, CH-1700 Fribourg, Switzerland

Supplimentary Information

Table of Contents

1. Synthesis of hydroxylamine derivatives

1.1 General

All the reagents were purchased from Sigma-Aldrich Co. LLC (Merck KGaA, Darmstadt, Germany) unless described, and purified as described when needed. Solvents and HPLC-grade solvents were purchased respectively from Acros Organic (Thermo Fischer Scientific, Inc., Geel, Belgium) and Sigma-Aldrich Co. LLC (Merck KGaA), and dried by solvent system (Innovative Technology Inc., FL, USA) or distilled when needed. Water was purified by Millipore purification system (Merck KGaA). Column chromatography and analytical TLC were performed on SILICYCLE SilicaFlash® F60 (230 – 400 mesh) and Silica gel 60 F254 TLC (Merck KGaA), respectively.

NMR spectra were recorded on a Bruker 400 spectrometer (Bruker BioSpin GmbH, Rheinstetten, Germany). HRMS were recorded on Bruker SolariX-FTICR 9.4 T MS (Bruker Daltonics, Bremen, Germany). FT-IR spectra were recorded on a JASCO 4100 FT-IR Spectrometer equipped with an ATR Pro One (JASCO, Inc., Tokyo, Japan). HPLC analyses were carried out using JASCO PU-2080 Plus HPLC pump, JASCO MD-2018 Plus detector, and ChromNAV Chromatography Data System (JASCO, Inc.).

1.2 Synthesis of hydroxylamine (HA)-peptide (apoB100-mimetic peptide) 1

Scheme S1. Synthesis of HA-peptide **1**.

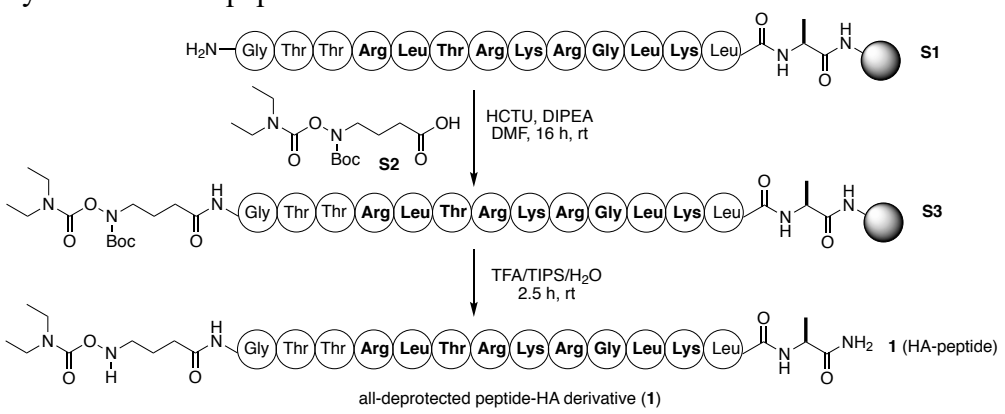

Peptide on resin S1. Peptide **S1** was synthesized by solid phase peptide synthesis (SPPS) using Rink-amide-MBHA resin (1.0 g, 0.52 mmol•g^{-1}, 1.0 equiv, Chem-Impex, Wood Dale, IL, USA). The resin was initially allowed to swell in CH_2Cl_2 for 20 min before adding 20% (v/v) piperidine in DMF (15 mL) to remove the Fmoc group on the resin. Separately, DIPEA (0.9 mL, 5.2 mmol, 10 equiv) was added to a solution of an *N*-Fmoc amino acid (2.6 mmol, 5 equiv) and HCTU (1.075 g, 2.6 mmol, 5 equiv) in a minimal amount of DMF. After stirring for 5 min, an activated *N*-Fmoc amino acid solution was added to the deprotected resin above. The reaction mixture was shaken for 1 h at room temperature. The resin was subsequently washed with DMF (15 mL, 3 times) and CH_2Cl_2 (15 mL, 3 times). The unreacted free amine groups on the resin were capped with a solution of acetic anhydride 20% (v/v) in the presence of DIPEA 20% (v/v) in DMF by shaking for 20 min at room temperature. The Fmoc group of the *N*-terminus of the peptide was deprotected by 20% (v/v) piperidine in DMF for the addition of the next Fmoc-amino acid. This protocol was repeated to obtain the peptide on resin **S1**.

***N*-Boc-HA-peptide on resin S3.** To a solution of HA-COOH linker **S2**[1] (0.5 g, 1.56 mmol, 3.0 equiv) and HCTU (0.64 g, 1.56 mmol, 3.0 equiv) in the minimal amount of DMF, DIPEA (0.55 mL, 3.12 mmol, 6.0 equiv) was added. After stirring for 5 min, the reaction mixture was added to the peptide on resin **S1** and shaken for 1 h at room temperature. The resin was washed with DMF (15 mL, 3 times) and CH_2Cl_2 (15 mL, 3 times) to obtain peptide **S3** on resin.

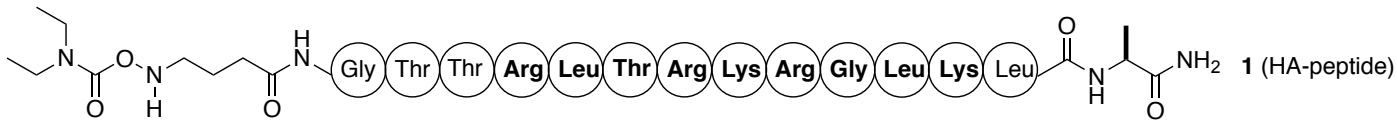

HA-peptide 1. To the HA-functionalized peptide on resin **S3** (0.5 g), a mixture of TFA/TIPS/H_2O (95:2.5:2.5 (v/v/v), 5.0 mL) was added and the reaction mixture was stirred for 2.5 h at room temperature. The reaction mixture was filtered to remove the resin and the filtrate was concentrated under reduced pressure. The peptide, which was deprotected and cleaved from the resin, was collected by precipitation with Et_2O. After centrifuge, the supernatant was removed and the precipitate (crude peptide) was dried under vacuum and purified by a reverse phase HPLC (column: Shiseido Capcell Pak C18 column (Φ 30

1. Oriana, S.; Fracassi, A.; Archer, C.; Yamakoshi, Y. Covalent surface modification of lipid nanoparticles by rapid potassium acyltrifluoroborate amide ligation. *Langmuir* **2018**, *34*, 13244 – 13251.

mm x 250 mm) (Shiseido Co. Ltd., Tokyo, Japan), solvent system: CH_3CN-H_2O in the presence of 0.1% TFA (a gradient of CH_3CN-H_2O (v/v, 10:90 to 90:10) over 40 min). The corresponding fraction was collected and its purity was confirmed by analytical reverse phase HPLC (Figure S1). The collected fraction was lyophilized to provide the all-deprotected peptide **1** (0.17 g, 0.096 mmol, 37% yield in total for peptide synthesis); HRMS (MALDI$^+$, matrix: HCCA) *m/z*: $[M+H]^+$calcd for $C_{76}H_{145}N_{28}O_{20}^+$: 1770.1184, found 1770.1185.

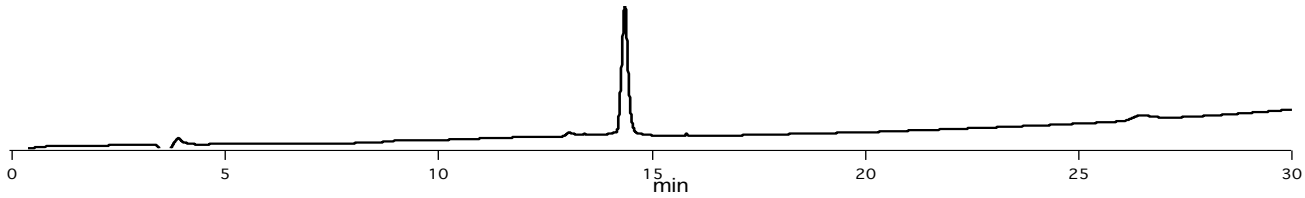

Figure S1. HPLC diagram of the purified HA-peptide (**HA-P**) **1** (column: Shiseido Capcell Pak C18 column (Φ 4.6 mm x 250 mm), solvent system: CH_3CN-H_2O with 0.1% TFA and a gradient of CH_3CN-H_2O (10:90 to 98:2, over 30 min), flow rate: 1 mL/min, detection: 220 nm).

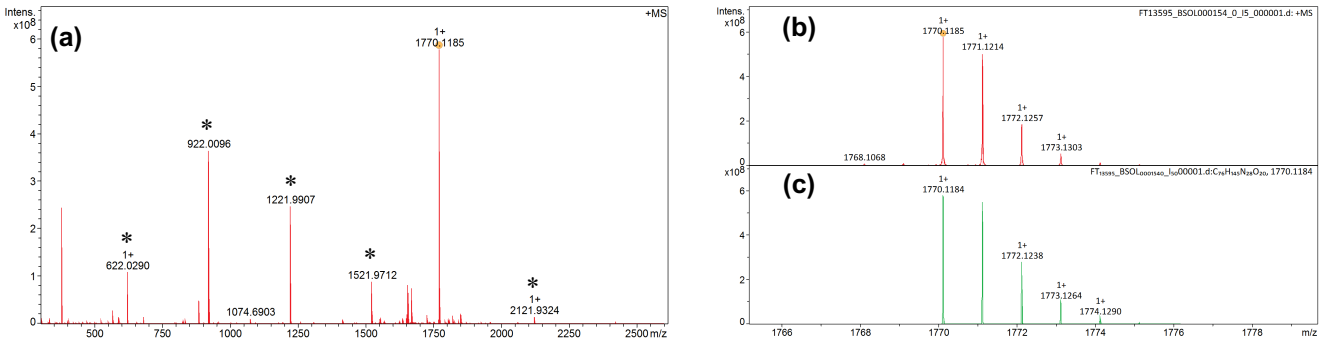

Figure S2. Positive HR-MALDI-MS (matrix: HCCA) of purified HA-peptide (**HA-P**) **1** (a), expansion of the molecular ion peaks (b) and their simulation (c). *The peaks for the calibration standards.

1.3 Preparation of HA-amine linker S5

Scheme S2. Synthesis of HA-NH_2 linker **S5**.

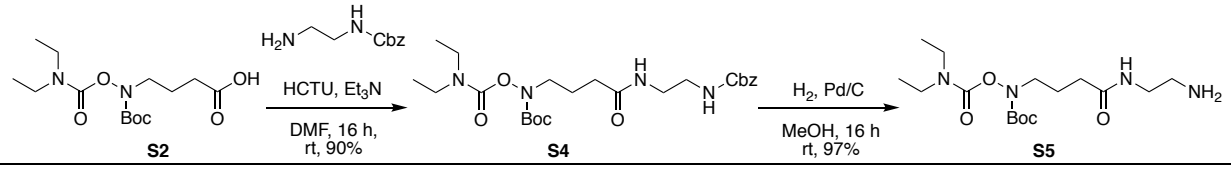

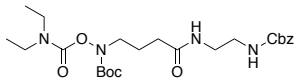

***tert*-Butyl(4-((2-(((benzyloxy)carbonyl)amino)ethyl)amino)-4-oxobutyl)((diethylcarbamoyl)oxy) carbamate (S4).** Compound **S2**[1] (200 mg, 0.63 mmol, 1.0 equiv), Et_3N (270 µL, 1.9 mmol, 3.0 equiv) and HCTU (260 mg, 0.63 mmol, 1.0 equiv) were dissolved in 5 mL of DMF. After stirring the reaction mixture for 5 min at room temperature, benzyl (2-aminoethyl) carbamate (220 mg, 0.72 mmol, 1.1 equiv) was added and the reaction mixture was stirred overnight at room temperature. After the removal of DMF under reduced pressure, the crude mixture was extracted by CH_2Cl_2 and purified by a silica gel column chromatography (solvent: hexane-EtOAc) to provide **S4** as a colorless oil (290 mg, 0.57 mmol, Y = 90%); IR (cm^{-1}): 3330 (N–H), 2977 (C–H), 2937 (C–H), 1718 (C=O), 1655, 1534 (C–N), 1423, 1367, 1264, 1144, 844, 1037, 845, 743, 698; ^{1}H NMR (400 MHz, in $CDCl_3$): δ 1.13 (m, $CH_2C\mathbf{H_3}$, 6 H), 1.38 (s, $C(C\mathbf{H_3})_3$, 9 H), 1.84 (quin, $CH_2C\mathbf{H_2}CH_2$, J = 6.5 Hz, 2H), 2.25 (t, $COC\mathbf{H_2}CH_2$, J = 7.1 Hz, 2H), 3.27 (m, $CONHC\mathbf{H_2}C\mathbf{H_2}$, $OCONHC\mathbf{H_2}$, 8H), 3.58 (t, $N(Boc)C\mathbf{H_2}$, J = 6.2 Hz, 2H), 5.04 (s, $OC\mathbf{H_2}Ph$, 2H) 5.78 (br.t, $CH_2N\mathbf{H}Cbz$, 1H), 6.52 (br.t, $CON\mathbf{H}CH_2$, 1H), 7.31 (m, Ph, 5H); ^{13}C NMR (100 MHz, in $CDCl_3$): δ 13.3, 14.2, 23.6, 28.1, 33.3, 38.6, 39.9, 41.2, 41.68, 43.1, 49.2, 66.6, 82.2, 128.0, 128.2, 128.4, 136.6, 154.3, 155.5, 156.9, 173.3; HRMS (ESI^+) *m/z*: $[M+H]^+$ calcd for $C_{24}H_{39}N_4O_7^+$, 495.2813; found, 495.2819.

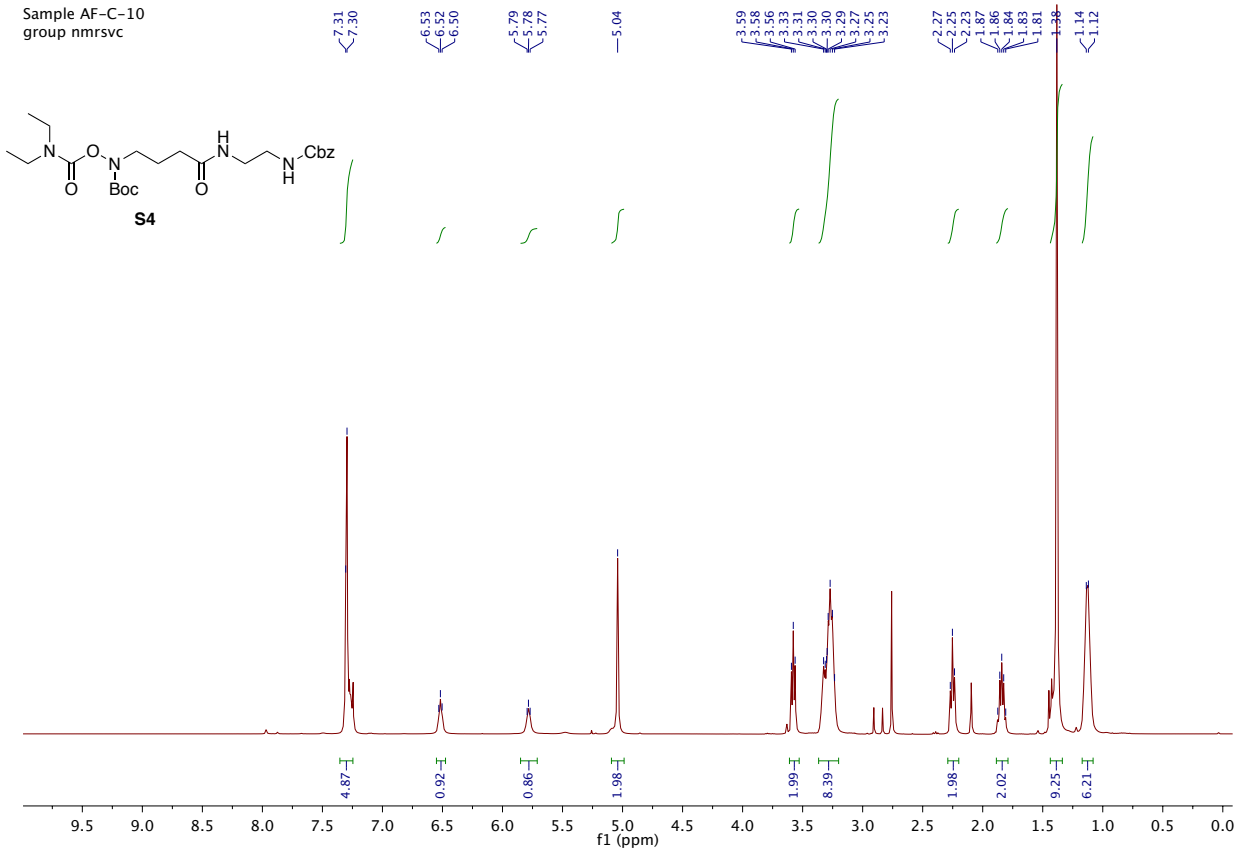

Figure S3. ^{1}H NMR spectrum of **S4** (in $CDCl_3$, 400 MHz).

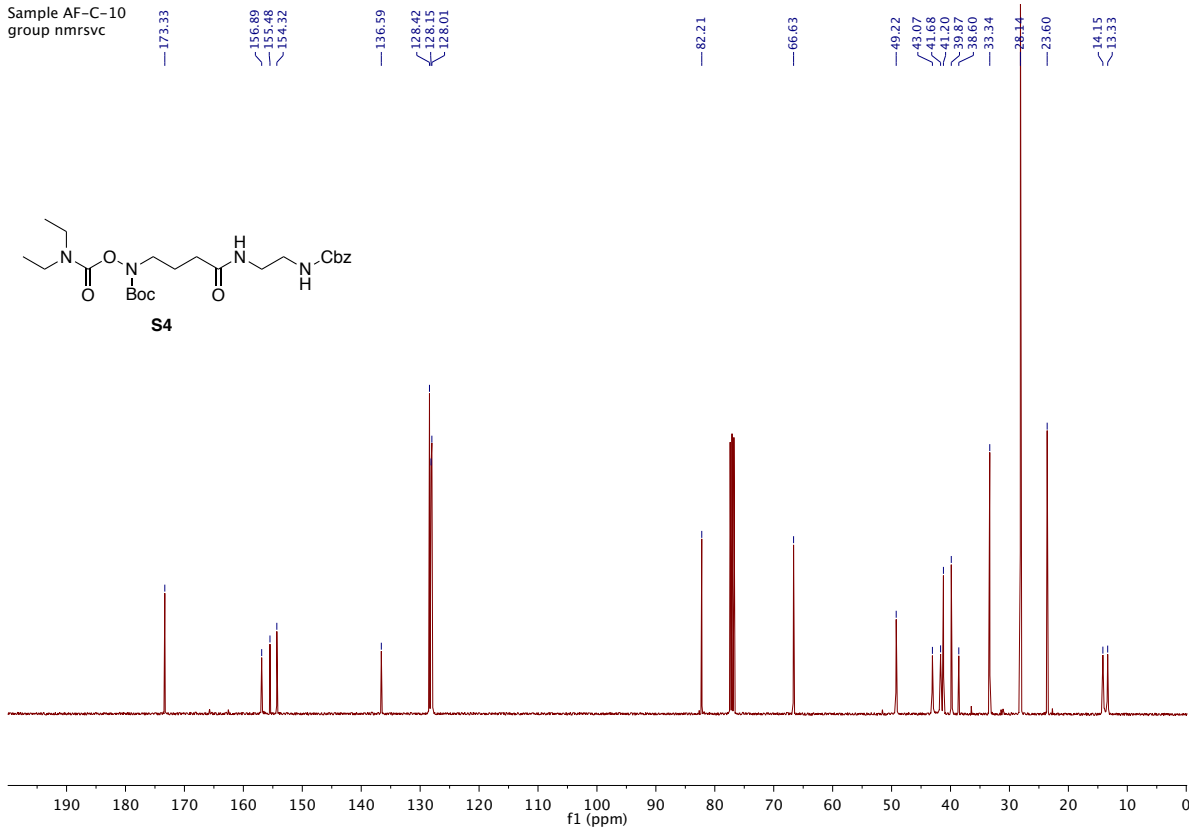

Figure S4. ^{13}C NMR spectrum of **S4** (in $CDCl_3$, 100 MHz).

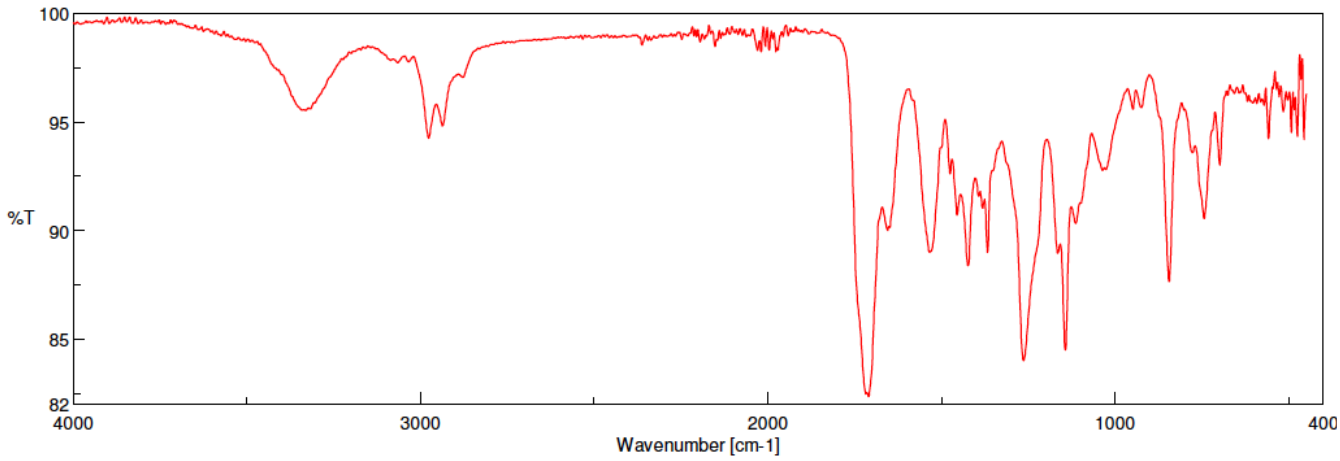

Figure S5. FT-IR ATR spectrum of **S4**.

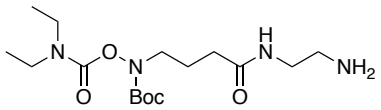

S5

***tert*-Butyl (4-((2-aminoethyl)amino)-4-oxobutyl)((diethylcarbamoyl)oxy)carbamate (S5).** Compound **S4** (400 mg, 0.8 mmol, 1.0 equiv) was dissolved in MeOH (10 mL) in a Schlenk flask and 10% Pd/C (wt/wt) (20 mg, 0.019 mmol, 0.024 equiv) was added. The mixture was stirred under H_2 atmosphere at room temperature for 16 h until completion of the reaction. Subsequently, EtOAc (10 mL) was added and

the mixture was filtered on a pad of celite. The solvent was removed under reduced pressure and the crude product **S5** (280 mg, 0.78 mmol, Y = 97% in crude) was used without any further purification; IR (cm^{-1}): 2979 (C–H), 2938 (C–H), 1727 (C=O), 1675 (C=O), 1541 (C–N), 1424, 1368, 1269, 1201, 1171, 1140, 928, 835, 798, 746, 721; ^{1}H NMR (400 MHz, in $CDCl_3$): δ 1.13 (m, $CH_2C\mathbf{H_3}$, 6 H), 1.41 (s, $C(C\mathbf{H_3})_3$, 9 H), 1.86 (quin, $CH_2C\mathbf{H_2}CH_2$, J = 6.9 Hz, 2H), 2.27 (t, $COC\mathbf{H_2}CH_2$, J = 7.25 Hz, 2H), 2.81 (t, $CH_2C\mathbf{H_2}NH_2$, J = 5.8 Hz, 2H), 3.27 (m, $OCONHC\mathbf{H_2}$, 6H), 3.59 (t, $N(Boc)C\mathbf{H_2}$, J = 6.4 Hz, 2H), 6.71 (t, $CON\mathbf{H}CH_2$, J = 5.7 Hz, 1H); ^{13}C NMR (100 MHz, $CDCl_3$): δ 13.3, 14.1, 23.3, 28.2, 33.4, 41.3, 41.6, 41.6, 43.0, 49.5, 82.0, 154.3, 155.4, 173.3; HRMS (ESI^+) *m/z*: $[M+Na]^+$ calcd for $C_{16}H_{32}N_4O_5Na^+$, 383.2265; found, 383.2256.

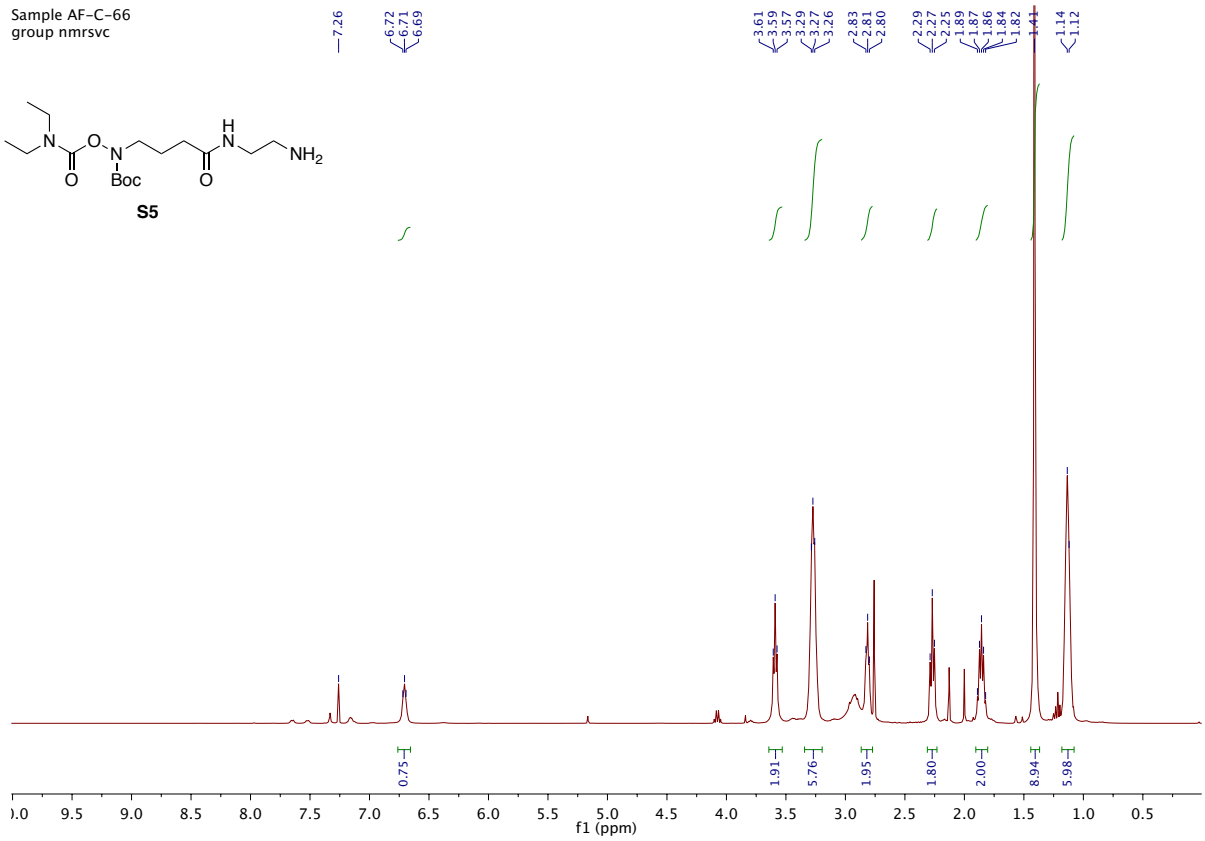

Figure S6. ^{1}H NMR spectrum of crude **S5** (in $CDCl_3$, 400 MHz).

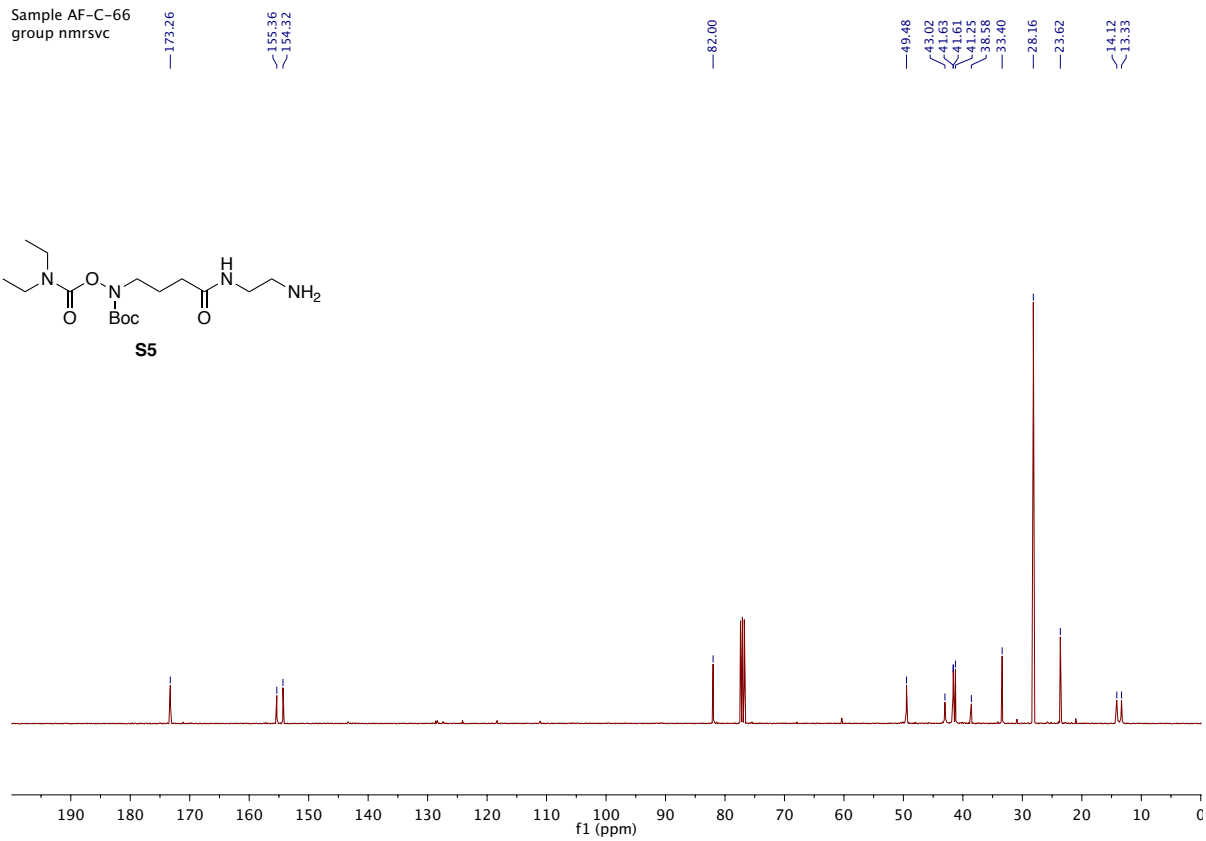

Figure S7. ^{13}C NMR spectrum of crude **S5** (in $CDCl_3$, 100 MHz).

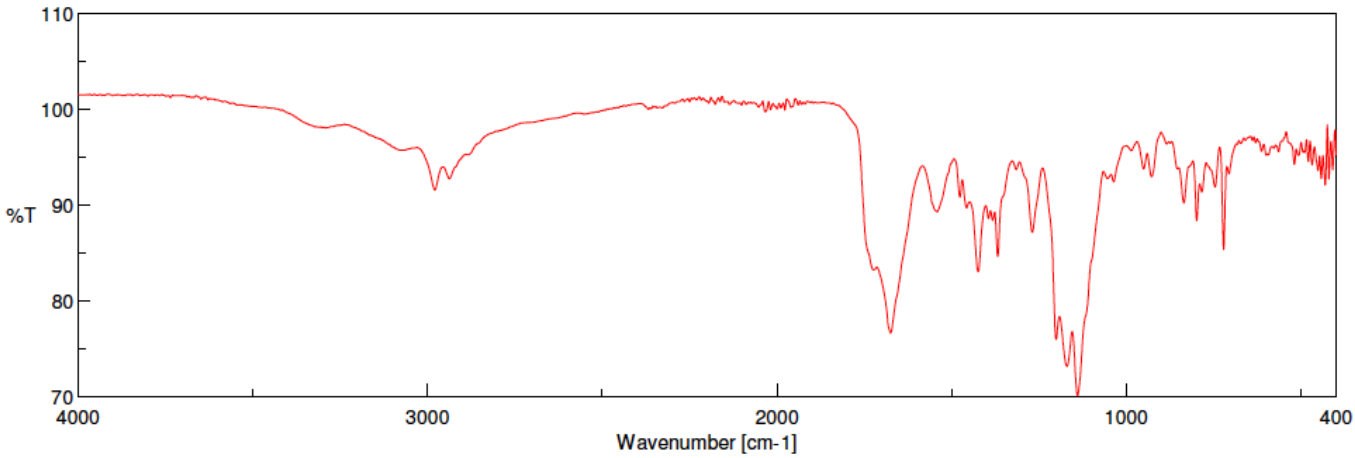

Figure S8. FT-IR ATR spectrum of crude **S5**.

1.4 Synthesis of HA-Gd(DO3A-MA) 2

Scheme S3. Synthesis of HA-Gd(DO3A-MA) **2**.

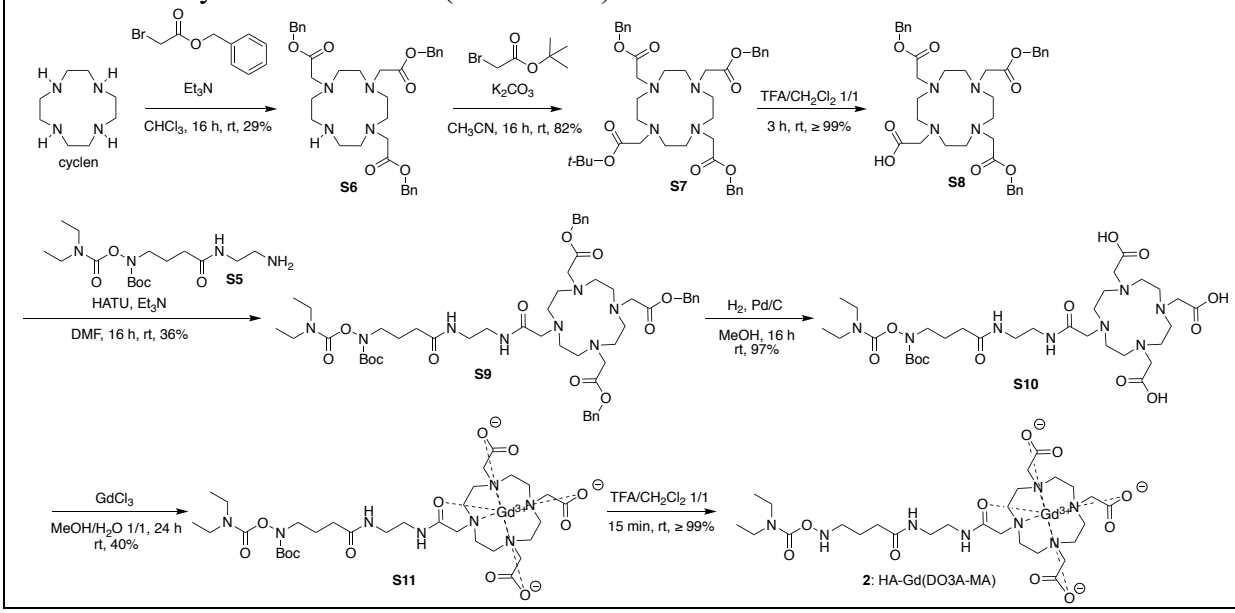

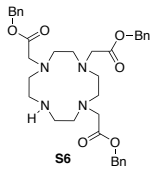

Tribenzyl 2,2',2''-(1,4,7,10-tetraazacyclododecane-1,4,7-triyl)triacetate (S6).[2] To a solution of cyclen (2.00 g, 11.6 mmol, 1.0 equiv, abcr GmbH, Karlsruhe, Germany) and Et_3N (5.86 g, 58 mmol, 5.0 equiv) in $CHCl_3$ (300 mL), a solution of benzyl bromoacetate (7.97 g, 34.8 mmol, 3.0 equiv) in $CHCl_3$ (50 mL) was added at 0 °C dropwise using a syringe pump over 30 min. After subsequently stirring overnight at room temperature, the solvent was removed and a crude mixture was extracted with CH_2Cl_2. The crude extract was purified by a silica column chromatography using CH_2Cl_2-MeOH as eluents to provide the colorless oil **S6** (2.07 g, 3.36 mmol, Y = 29%); ^{1}H NMR (400 MHz, in $CDCl_3$): δ 2.83-2.87 (m, C**H$_2$**NCH$_2$COO, 12 H), 3.07 (t, NHC**H$_2$**, *J* = 4.1 Hz, 4 H), 3.40 (s, NC**H$_2$**COO, 2 H,), 3.47 (s, NC**H$_2$**COO, 4 H), 5.12 (s, OC**H$_2$**Ph, 6 H), 7.33 (m, Ph, 15 H); ^{13}C NMR (100 MHz, $CDCl_3$): δ 47.4, 48.7, 49.5, 51.6, 51.8, 57.3, 66.7, 128.5, 128.6, 128.6, 128.7, 128.8, 135.4, 135.4, 170.2, 171.0; HRMS (ESI$^+$) *m/z*: $[M+H]^+$ calcd for $C_{35}H_{45}N_4O_6^+$, 617.3334; found, 617.3338.

2. Karfeld, L. S.; Bull, S. R.; Davis, N. D.; Meade, T. J.; Barron, A. E. Use of a genetically engineered protein for the design of a multivalent MRI contrast agent. *Bioconjugate Chem.*, **2007**, *18*, *6*, 1696-1700.

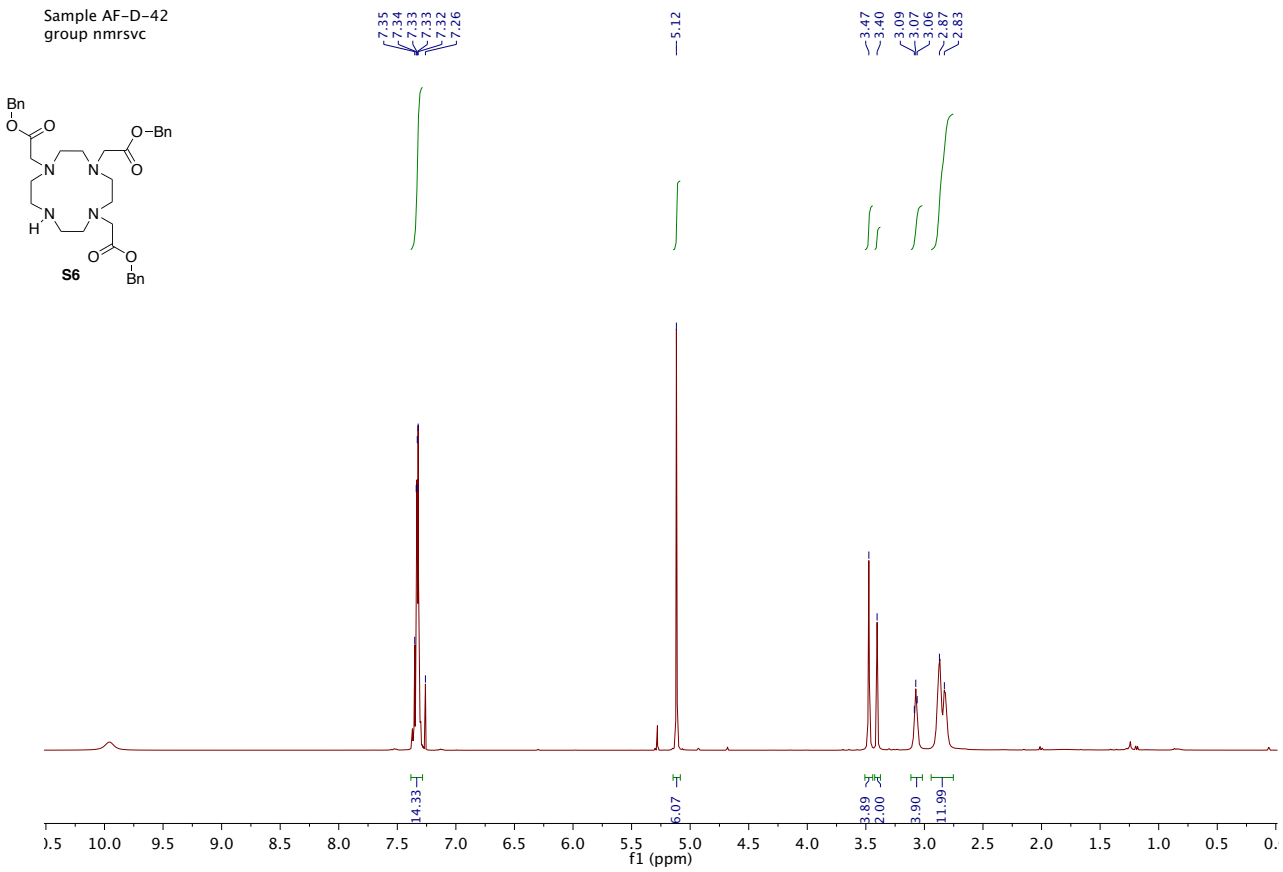

Figure S9. ^{1}H NMR spectrum of **S6** (in $CDCl_3$, 400 MHz).

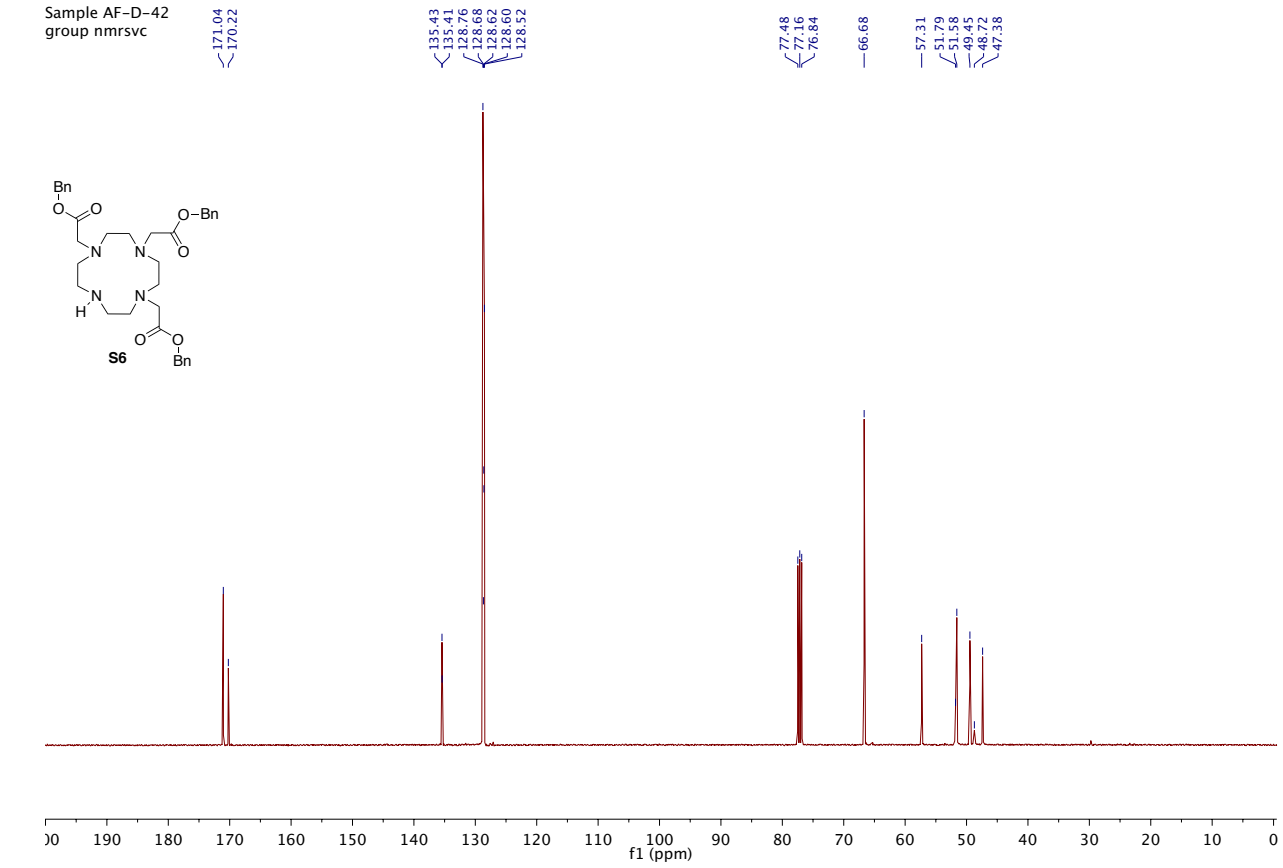

Figure S10. ^{13}C NMR spectrum of **S6** (in $CDCl_3$, 100 MHz).

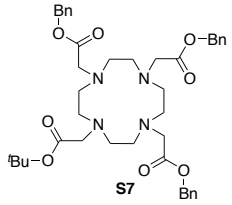

Tribenzyl 2,2',2''-(10-(2-(*tert*-butoxy)-2-oxoethyl)-1,4,7,10-tetraazacyclododecane-1,4,7-triyl)triacetate (S7).[3] To a solution of **S6** (2.0 g, 3.3 mmol, 1.0 equiv) in 40 mL of CH_3CN, K_2CO_3 (0.705 g, 5.0 mmol, 1.5 equiv) and *tert*-butyl bromoaceate (0.66 g, 3.3 mmol, 1.0 equiv) were added. The reaction mixture was stirred overnight at room temperature, filtered, and the solvent was removed under vacuum. The obtained crude mixture was purified by a silica column chromatography (CH_2Cl_2-MeOH) to provide compound **S7** as a colorless oil (1.97 g, 2.7 mmol, Y = 82%); ^{1}H NMR (400 MHz, in $CDCl_3$): δ 1.40 (s, C(C**H₃**)$_3$ 9 H), 2.95-4.12 (m, C**H₂**NC**H₂**COO 24 H), 5.02 (m, OC**H₂**Ph 6 H), 7.29 (m, Ph, 15 H); ^{13}C NMR (100 MHz, in $CDCl_3$): δ 28.1, 55.2, 55.4, 56.0, 66.9, 67.0, 82.1, 128.4, 128.5, 128.6, 128.6, 128.7, 135.3, 173.3, 173.78, 173.82; HRMS (ESI$^+$) *m/z*: $[M+Na]^+$ calcd for $C_{41}H_{54}N_4O_8Na^+$, 753.3834; found, 753.3829.

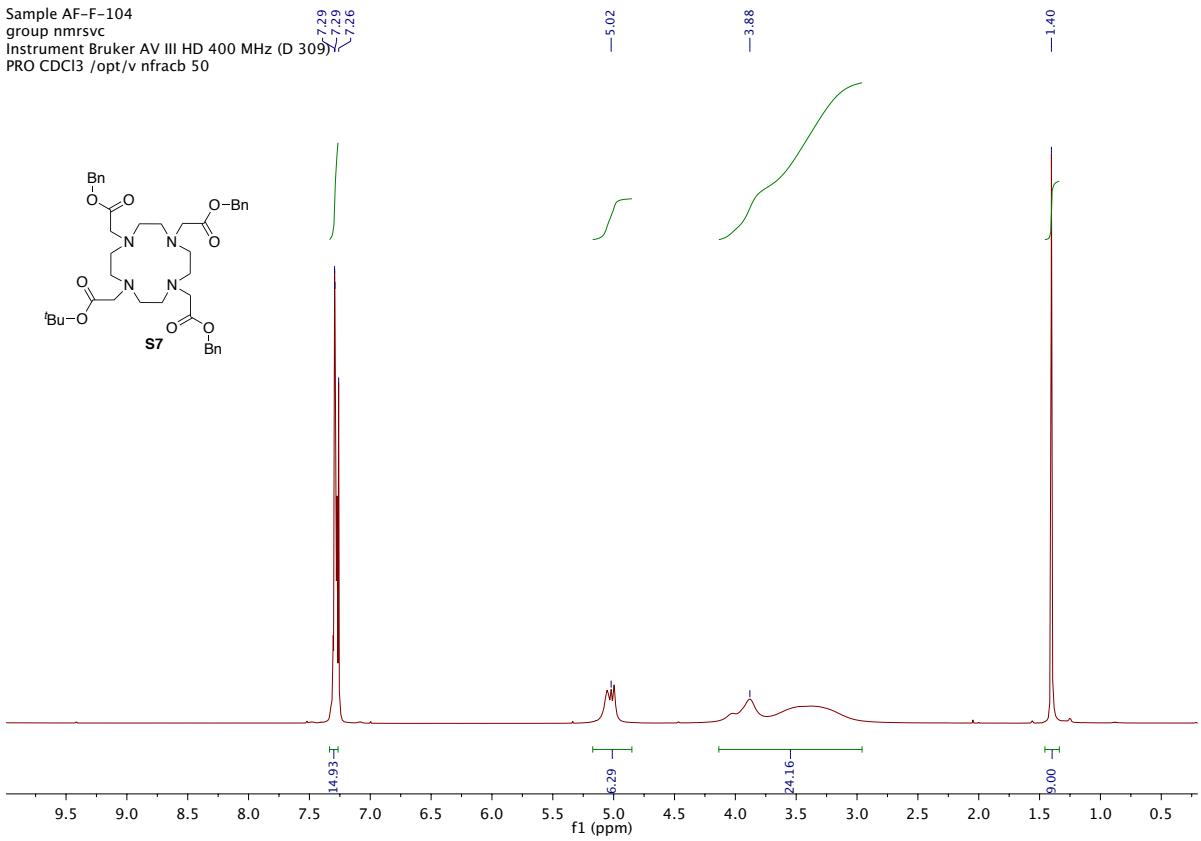

Figure S11. ^{1}H NMR spectrum of **S7** (in $CDCl_3$, 400 MHz).

3. Hu, H. Y.; Lim, N. H.; Pfennigdorff, D. D.; Saas, J.; Wendt, K. U.; Ritzeler, O.; Nagase, H.; Plettenburg, O.; Schultz, C.; Nazare, M. DOTAM Derivatives as active cartilage-targeting drug carriers for the treatment of osteoarthritis. *Bioconjugate Chem.*, **2015**, *26*, 383-388.

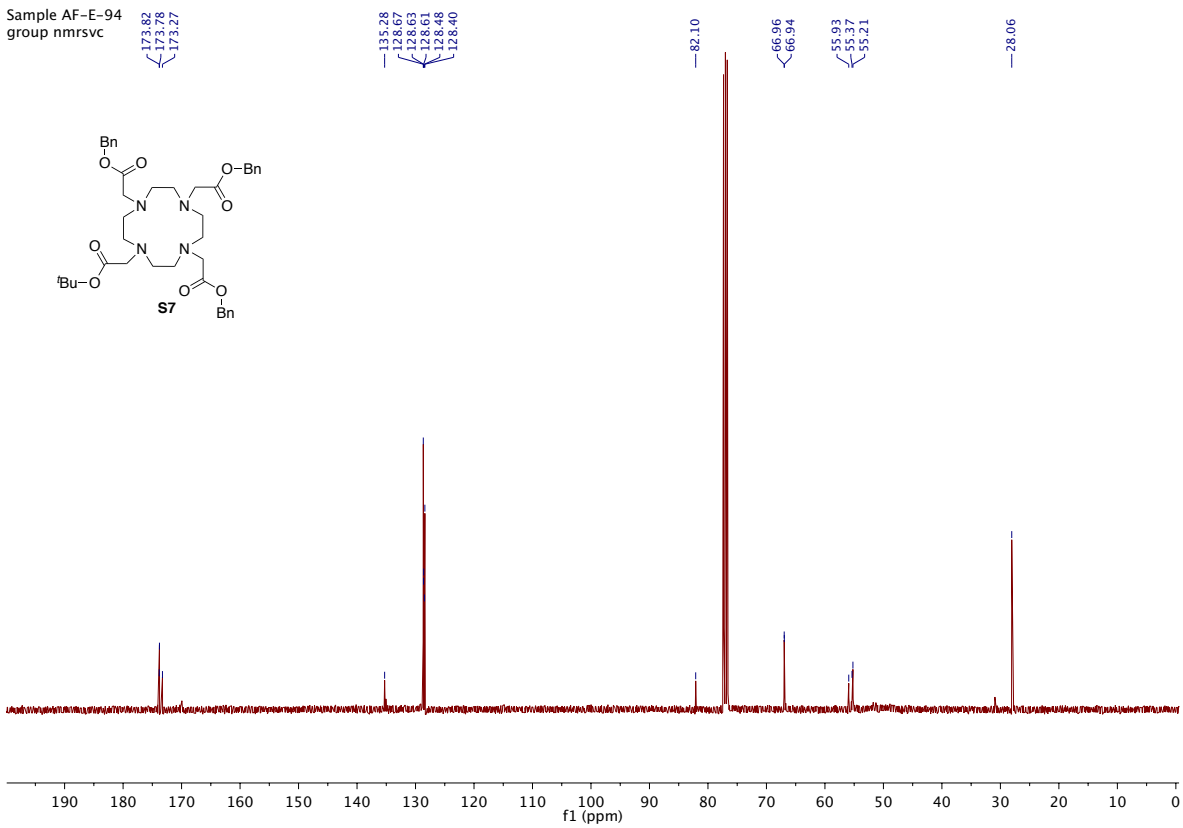

Figure S12. ^{13}C NMR spectrum of **S7** (in $CDCl_3$, 100 MHz).

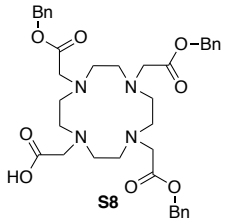

2-(4,7,10-Tris(2-(benzyloxy)-2-oxoethyl)-1,4,7,10-tetraazacyclododecan-1-yl)acetic acid (S8).[3] To a solution of compound **S7** (1.8 g, 2.46 mmol, 1.0 equiv) in CH_2Cl_2 (3 mL), TFA (3 mL) was added. The reaction mixture was stirred for 3 h at room temperature. The solvent was removed by a flux of N_2 to provide crude **S8** as a yellow oil (1.6 g, 2.6 mmol, Y ≥ 99%, the product was used without further purification); ^{1}H NMR (400 MHz, in DMSO-d_6): δ 1.91-3.74 (m, C**H$_2$**NC**H$_2$**COO, 24 H), 5.13 (m, OC**H$_2$**Ph, 6 H), 7.35 (m, Ph, 15 H); ^{13}C NMR (100 MHz, in DMSO-d_6): δ 55.4, 66.3, 66.4, 67.9, 128.5, 128.6, 128.6, 128.8, 128.8, 128.9, 128.9, 128.95, 128.99, 135.5, 136.2, 136.2, 158.0, 173.4; HRMS (ESI$^+$) *m/z*: $[M+H]^+$ calcd for $C_{37}H_{47}N_4O_8^+$, 675.3388; found, 675.3391.

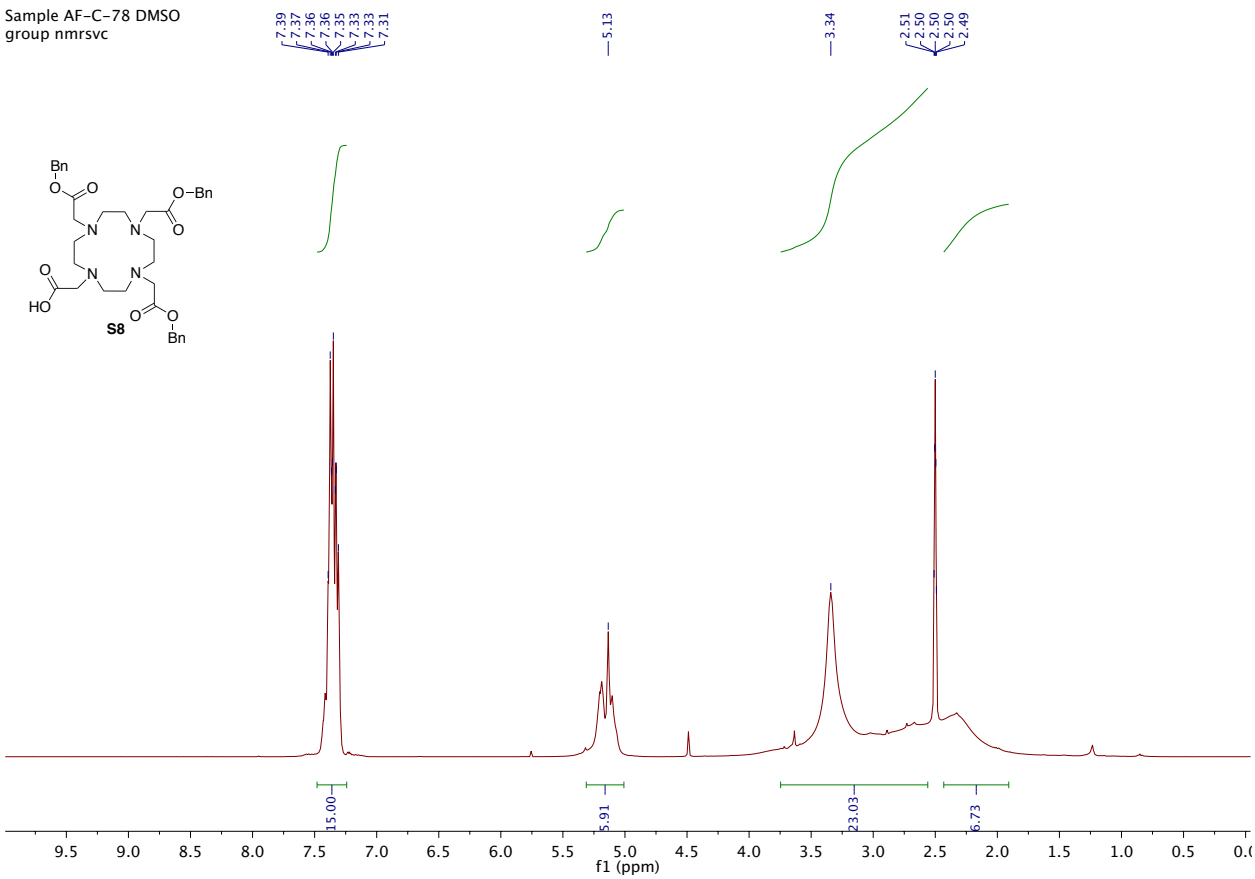

Figure S13. ^{1}H NMR spectrum of **S8** (in DMSO-d_6, 400 MHz).

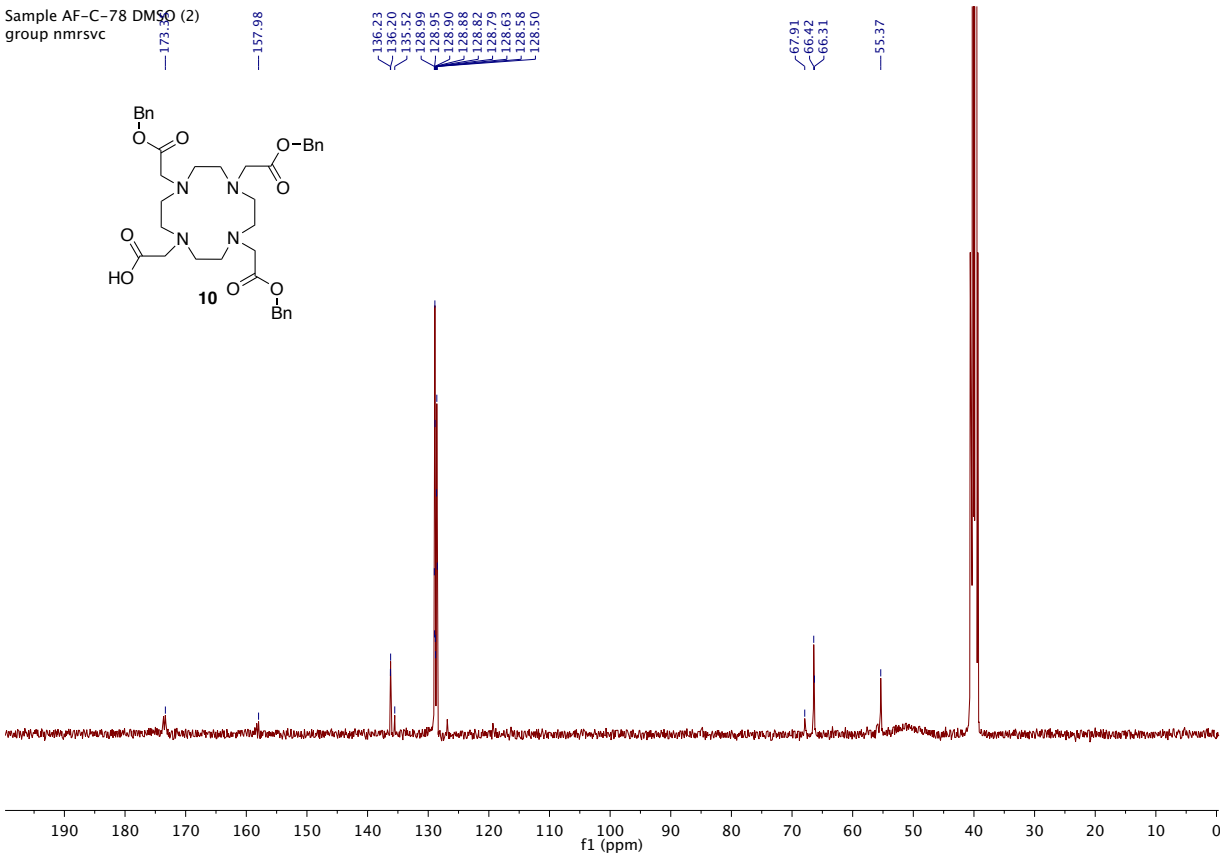

Figure S14. ^{13}C NMR spectrum of **S8** (in DMSO-d_6, 100 MHz).

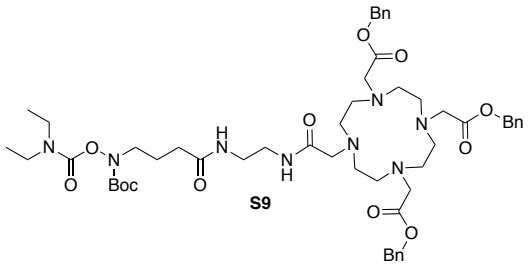

Tribenzyl2,2',2''-(10-(6-(*tert*-butoxycarbonyl)-3-ethyl-4,10,15-trioxo-5-oxa-3,6,11,14-tetraazahexadecan -16-yl)-1,4,7,10-tetraazacyclododecane-1,4,7-triyl)triacetate (S9). To a solution of compound **S8** (0.44 g, 0.65 mmol, 1.0 equiv) in DMF (10 mL), Et_3N (270 μL, 0.2 g, 1.95 mmol, 3.0 equiv) and HATU (0.247 g, 0.65 mmol, 1.0 equiv) were added. After stirring the solution for 5 min, compound **S5** (0.26 g, 0.72 mmol, 1.1 equiv) was added and the reaction mixture was stirred overnight at room temperature. After the removal of DMF, the crude mixture was extracted with CH_2Cl_2 and the obtained crude mixture was purified by a silica gel column chromatography (CH_2Cl_2-MeOH) to provide **S9** as a colorless solid (0.24 g, 0.23 mmol, Y = 36%); IR (cm^{-1}): 3091.3 (N–H), 2979 (C–H), 1736 (C=O), 1686 (C=O), 1556 (C–N), 1457, 1392, 1367, 1200, 1165, 1090, 797, 747, 698; ^{1}H NMR (400 MHz, in $CDCl_3$): δ 1.17 (m, $CH_2C\mathbf{H_3}$, 6 H), 1.45 (s, $C(C\mathbf{H_3})_3$, 9 H), 1.89 (quin, $CH_2C\mathbf{H_2}CH_2$, *J* = 6.85 Hz, 2H), 2.0-3.7 (m, $C\mathbf{H_2}NC\mathbf{H_2}COO$, $NC\mathbf{H_2}CH_3$, $N(Boc)C\mathbf{H_2}$, $NHC\mathbf{H_2}C\mathbf{H_2}NH$,$COC\mathbf{H_2}CH_2$, 34H), 5.13 (s, $OC\mathbf{H_2}Ph$, 2 H), 5.20 (s, $OC\mathbf{H_2}Ph$, 4 H), 6.43 (t, CON**H,** *J* = 5.9 Hz, 1H), 7.02 (t, CON**H,** *J* = 7.9 Hz, 1H), 7.31 (m, Ph, 15 H); ^{13}C NMR (100 MHz, $CDCl_3$): δ 13.4, 14.1, 23.2, 28.2, 32.9, 38.9, 39.7, 41.7, 43.0, 49.2, 55.2, 55.3, 55.5, 67.1, 82.0, 128.4, 128.5, 128.5, 128.6, 128.6, 128.7, 135.2, 135.4, 154.3, 155.5, 172.1, 173.3, 173.5; HRMS (ESI^+) *m/z*: $[M+Na]^+$ calcd for $C_{53}H_{76}N_8O_{12}Na^+$, 1039.5475; found, 1039.5470.

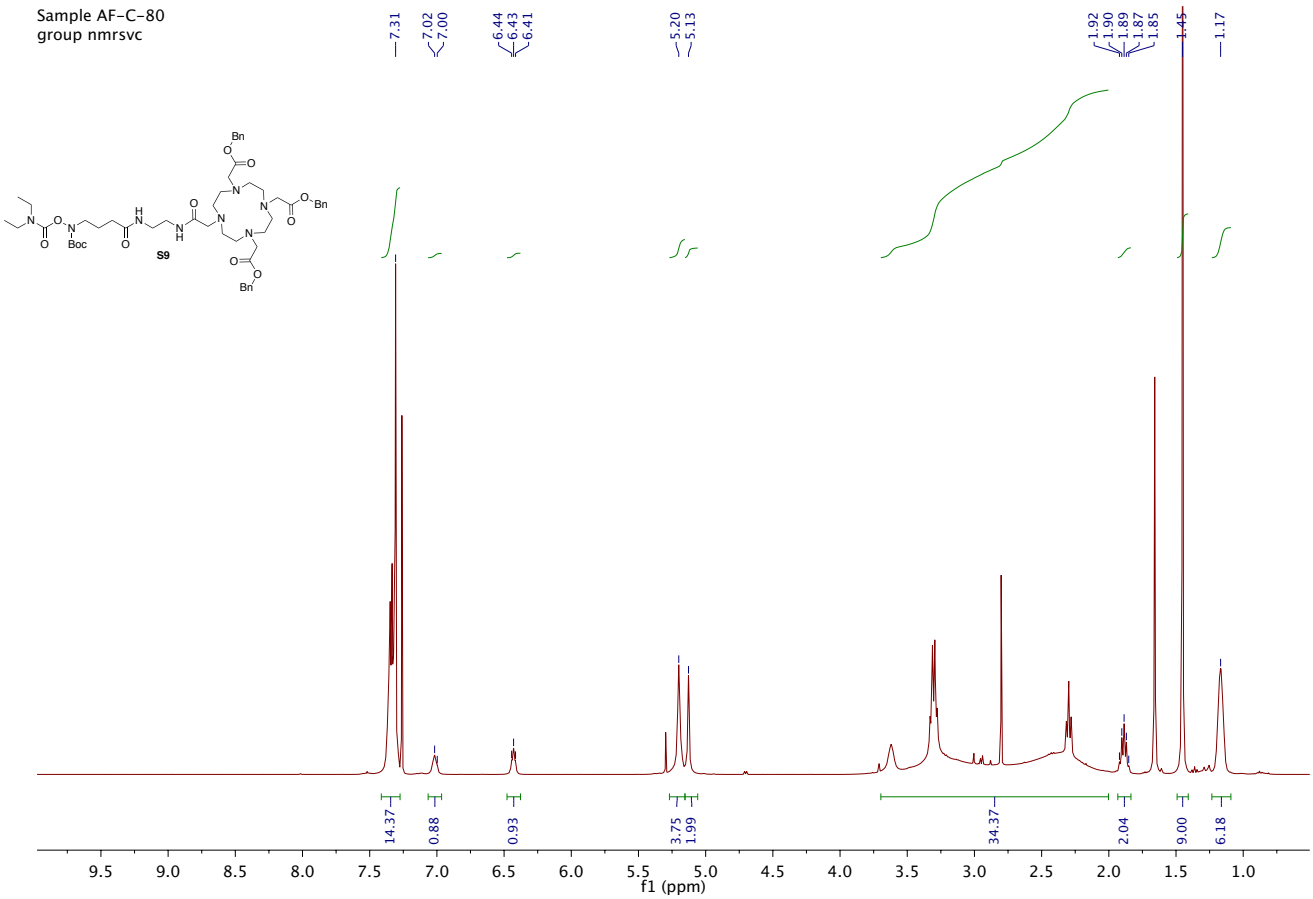

Figure S15. ^{1}H NMR spectrum of **S9** (in $CDCl_3$, 400 MHz).

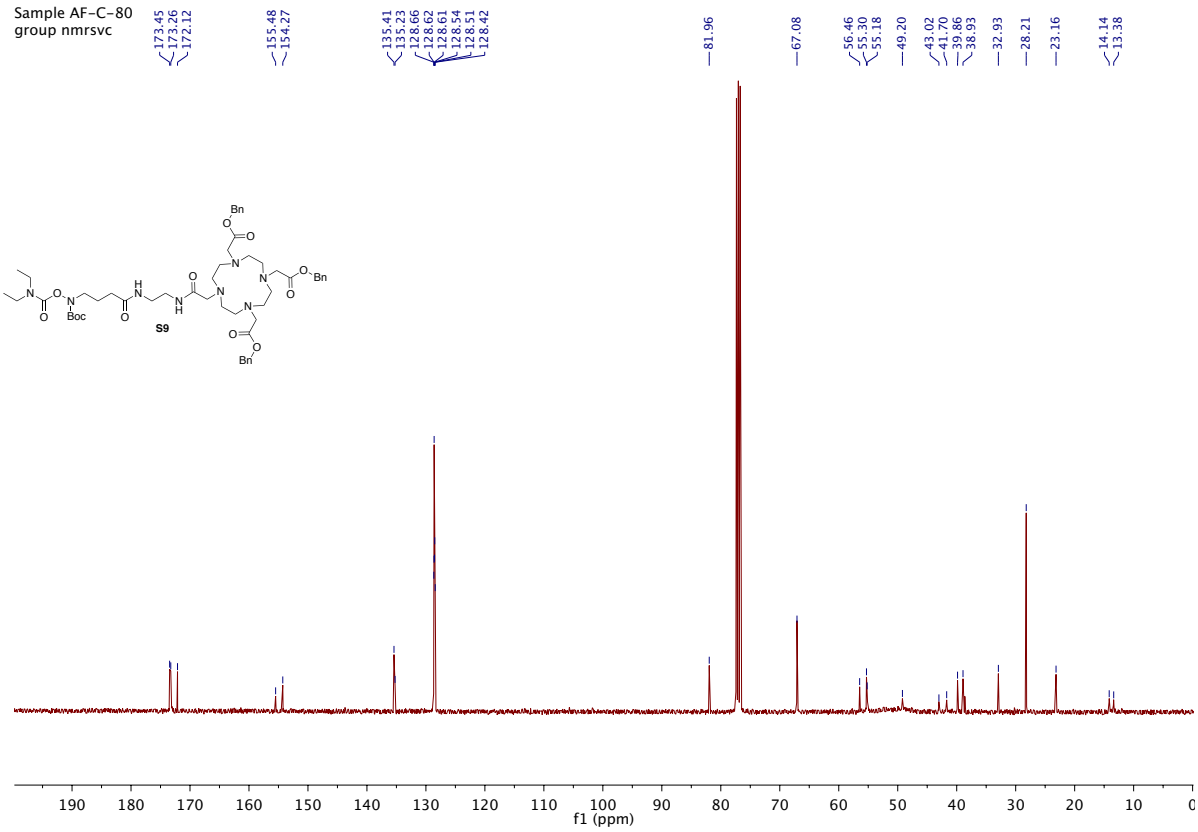

Figure S16. ^{13}C NMR spectrum of **S9** (in $CDCl_3$, 100 MHz).

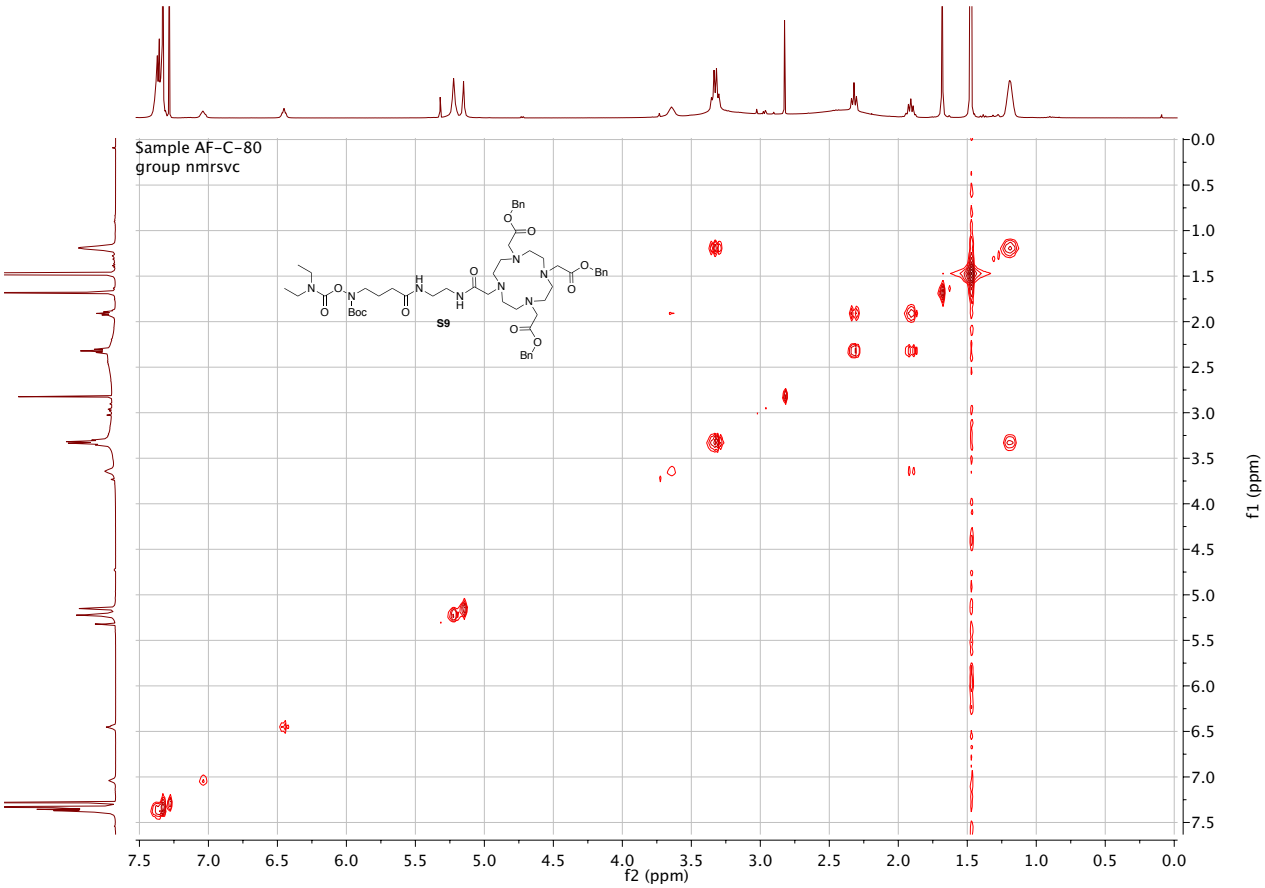

Figure S17. COSY spectrum of **S9** (in $CDCl_3$, 400 MHz).

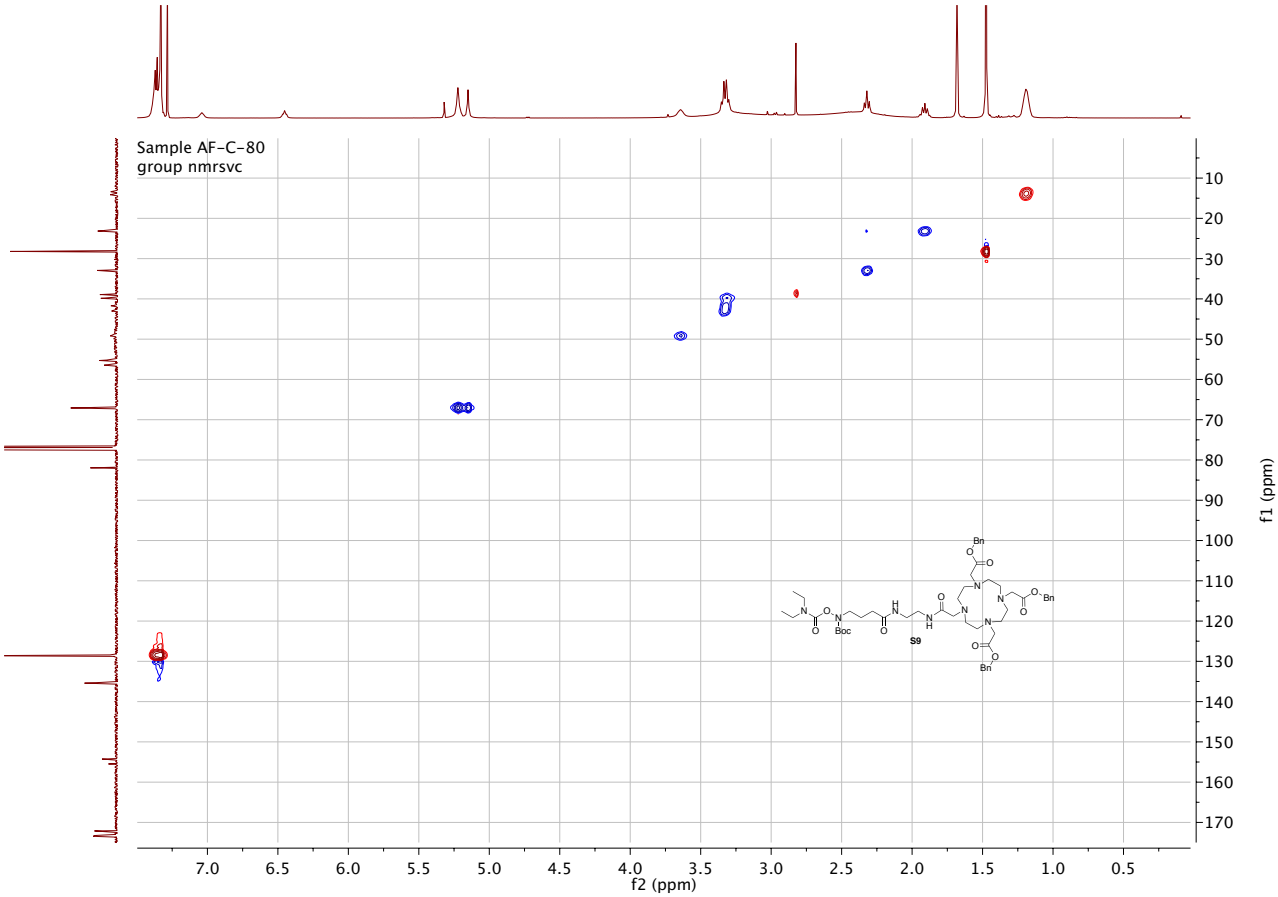

Figure S18. HSQC spectrum of **S9** (in $CDCl_3$).

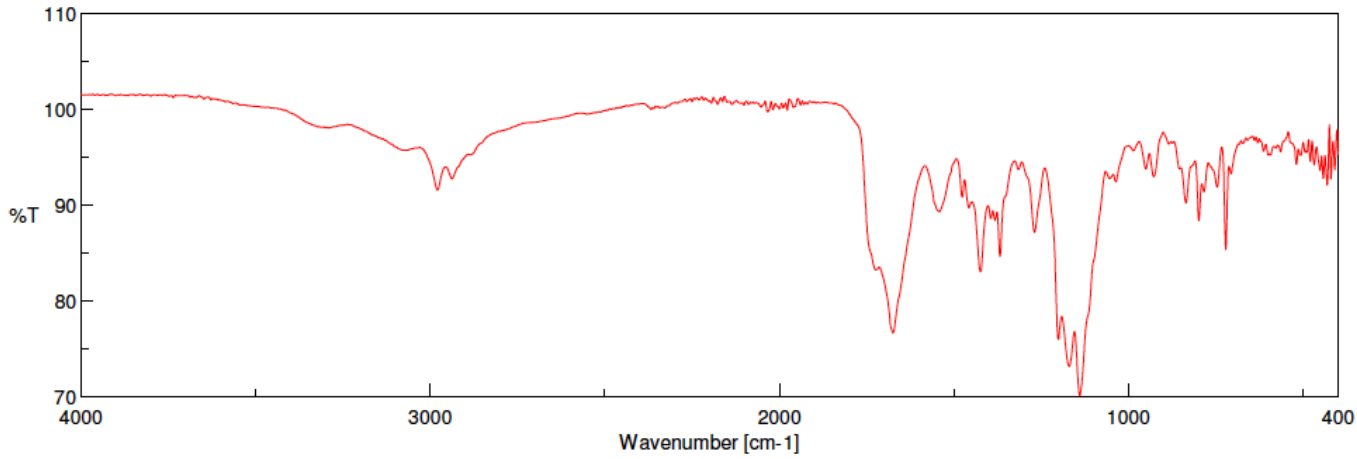

Figure S19. FT-IR ATR spectrum of **S9**.

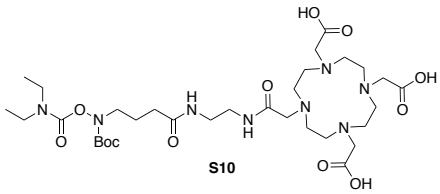

2,2',2''-(10-(6-(*tert*-Butoxycarbonyl)-3-ethyl-4,10,15-trioxo-5-oxa-3,6,11,14-tetraazahexadecan-16-yl)-1,4,7,10-tetraazacyclododecane-1,4,7-triyl)triacetic acid (S10). Compound **S9** (0.24 g, 0.24 mmol, 1.0 equiv) was dissolved in MeOH (10 mL) in a Schlenk flask and Pd/C (10%, wt.) (20 mg, 0.019 mmol, 0.08 equiv) was added. The reaction mixture was stirred under H_2 atmosphere at room temperature for 16 h until completion of the reaction. After addition of EtOAc (10 mL), the mixture was filtered on a pad of celite. The solvent was removed under reduced pressure to give the crude product **S10** (164 mg, 0.22 mmol, y = 91% in crude), which was used without any further purification; IR (cm^{-1}): 3323 (O–H), 3094 (N–H), 2980 (C–H), 1730 (C=O), 1670 (C=O), 1462, 1426.1, 1394, 1370, 1273, 1189, 1143, 798, 719; ^{1}H NMR (400 MHz, DMSO-d_6): δ 1.10 (m, $CH_2C\mathbf{H_3}$, 6 H), 1.38 (s, $C(C\mathbf{H_3})_3$, 9 H), 1.72 (quin, $CH_2C\mathbf{H_2}CH_2$, J = 6.87 Hz, 2H), 2.14 (t, $COC\mathbf{H_2}CH_2$, J = 7.19 Hz, 2H), 2.55-3.66 (m, $C\mathbf{H_2}NC\mathbf{H_2}COO$, $NC\mathbf{H_2}CH_3$, $N(Boc)C\mathbf{H_2}$, $NHC\mathbf{H_2}C\mathbf{H_2}NH$,$COC\mathbf{H_2}CH_2$, 34H); ^{13}C NMR (100 MHz, in DMSO-d_6): δ 13.8, 14.5, 23.5, 28.3, 32.7, 38.7, 41.6, 43.0, 49.9, 55.5, 81.4, 153.9, 154.9, 172.2; HRMS (ESI^+) *m/z*: $[M+H]^+$ calcd for $C_{32}H_{59}N_8O_{12}^+$ 747.4247; found, 747.4250.

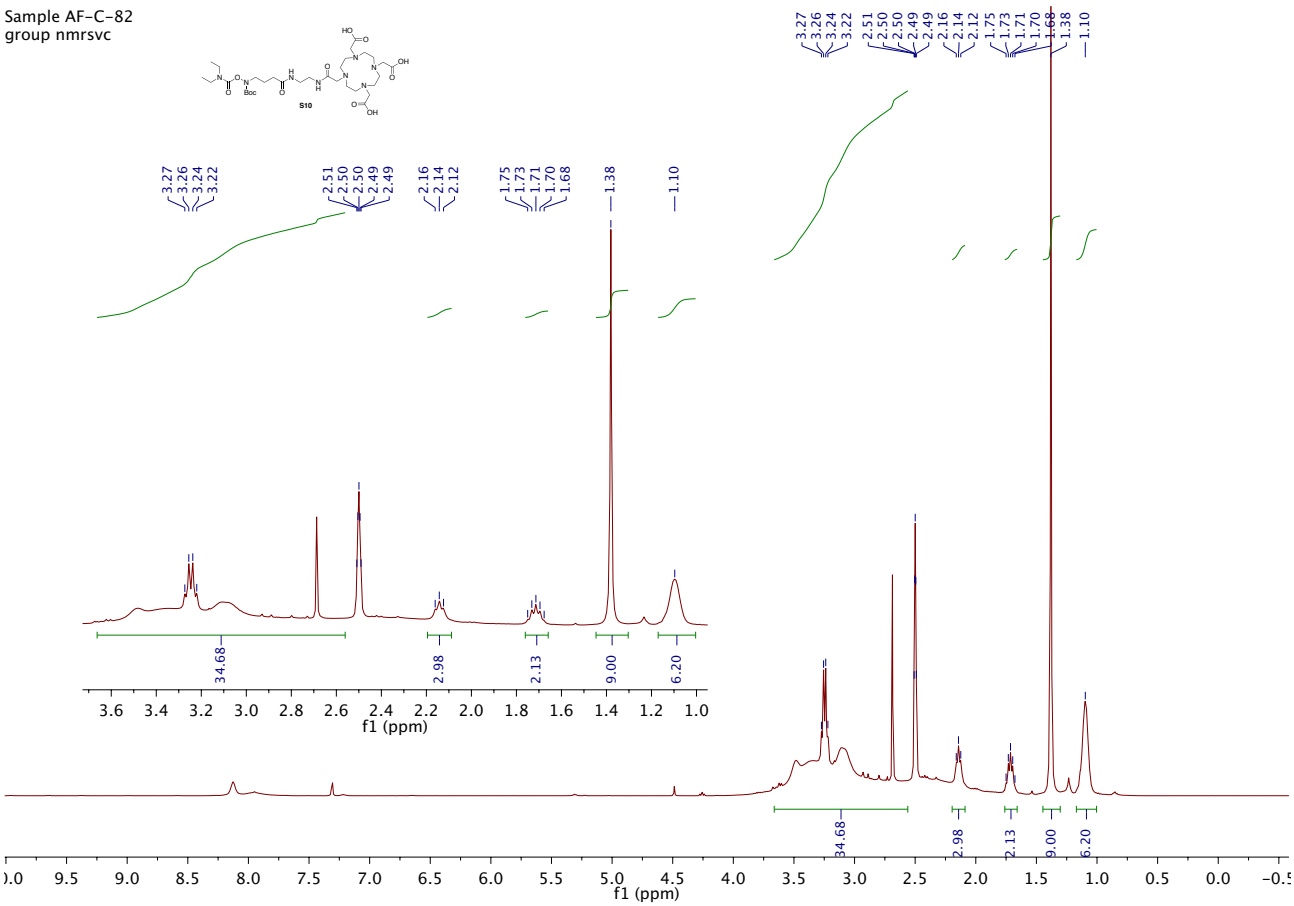

Figure S20. ^{1}H NMR spectrum of **S10** (in DMSO-d_6, 400 MHz).

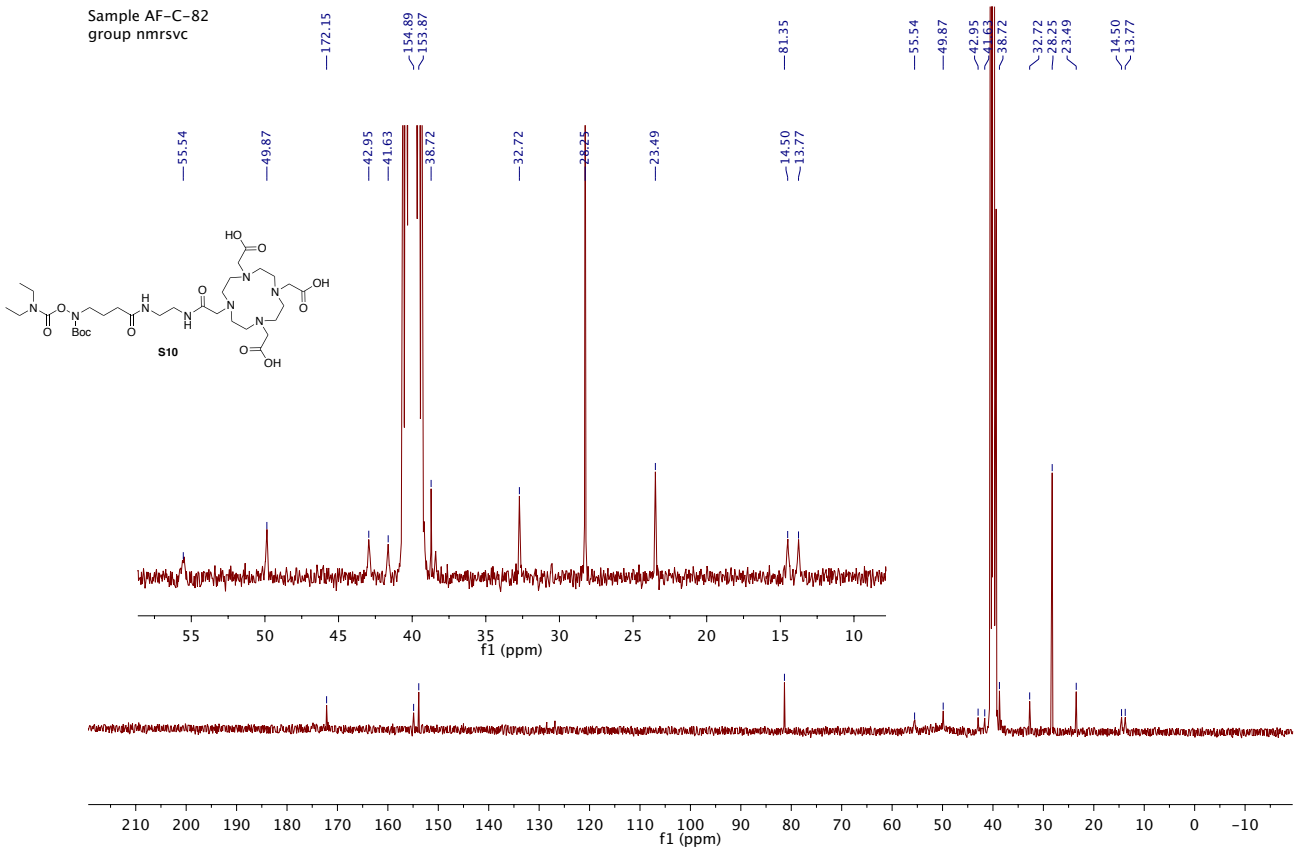

Figure S21. ^{13}C NMR spectrum of **S10** (in DMSO-d_6, 100 MHz).

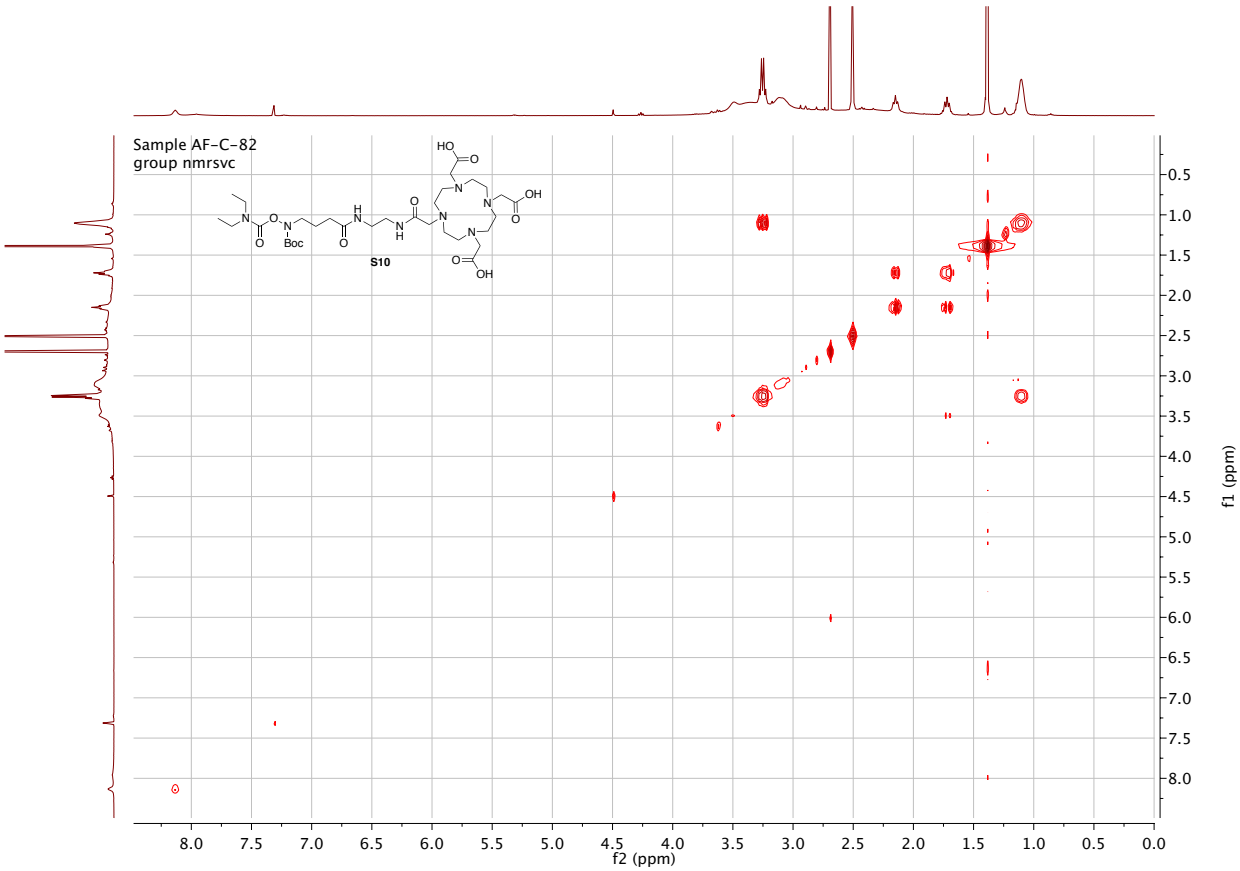

Figure S22. COSY spectrum of **S10** (in DMSO-d_6, 400 MHz).

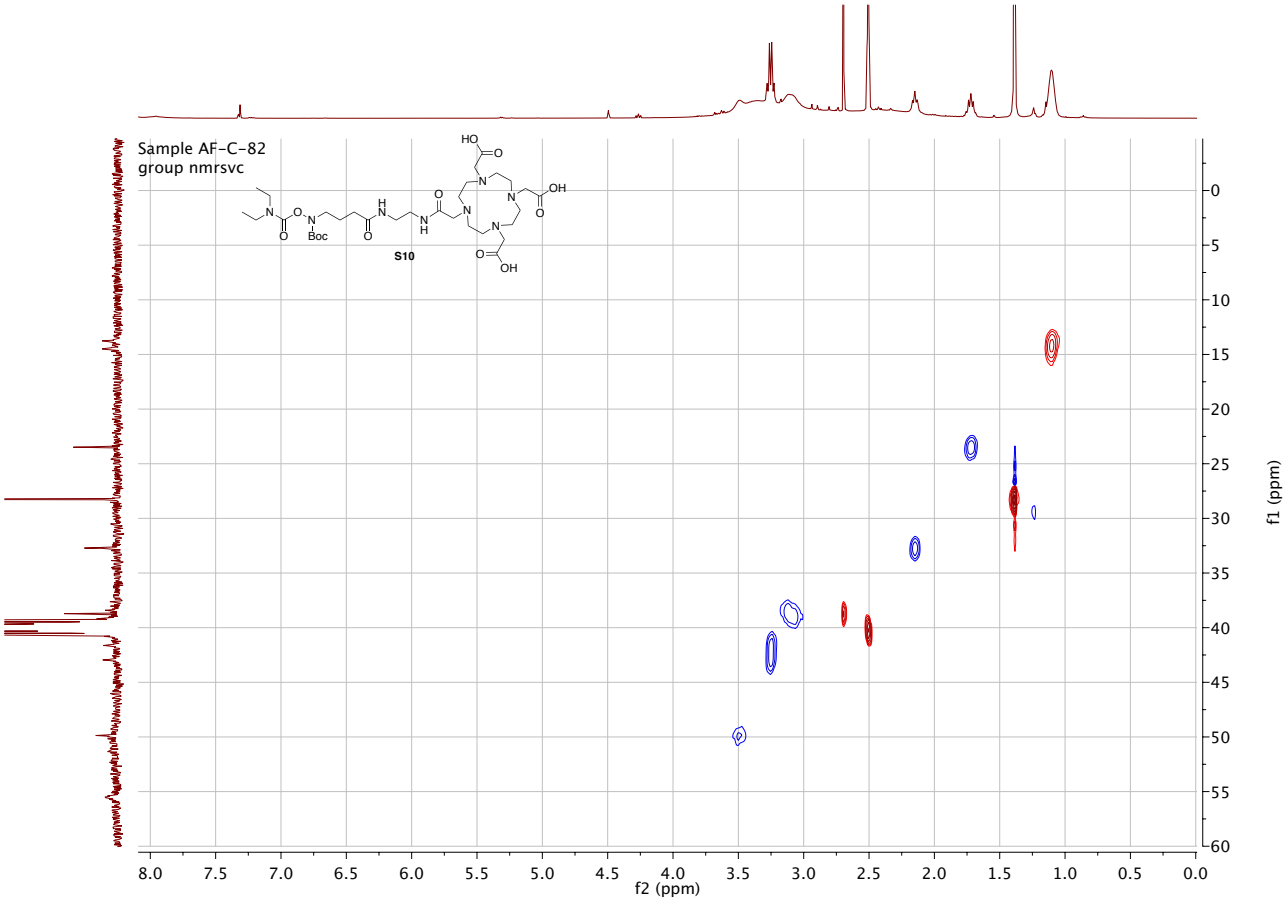

Figure S23. HSQC spectrum of **S10** (in DMSO-d_6).

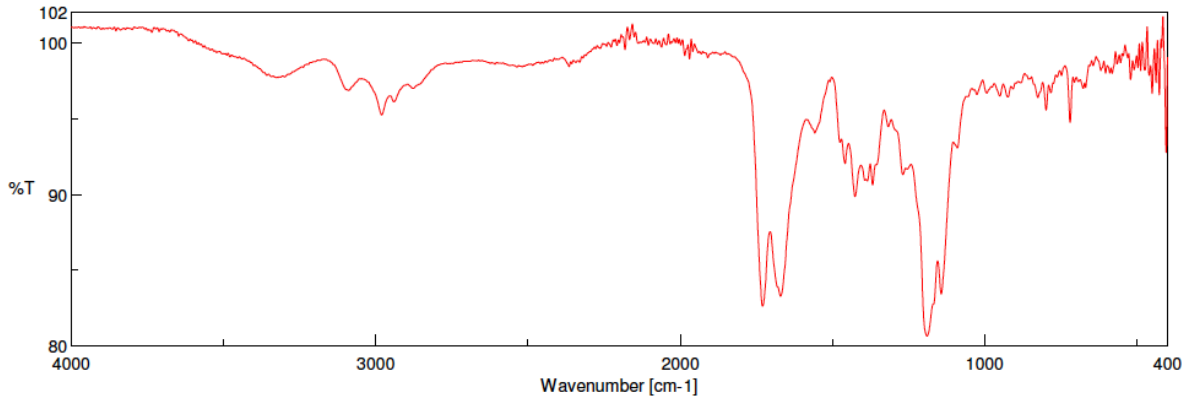

Figure S24. FT-IR ATR spectrum of **S10**.

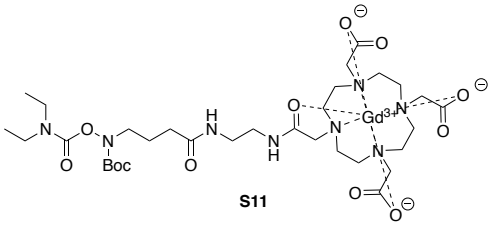

HA(Boc)-Gd(DO3A-MA) (S11). To a solution of compound **S10** (0.15 g, 0.20 mmol, 1.0 equiv) in MeOH (5 mL), a solution of $GdCl_3$ (0.058 mg, 0.22 mmol, 1,1 equiv, Alfa Aesar, Ward Hill, MA, USA) in water (5 mL) was added. The pH was slowly adjusted to 6.5 using 0.1 N NaOH. The reaction mixture was stirred for 24 h at room temperature. Subsequently, pH of the reaction mixture was adjusted to 9 using 0.1 N NaOH to remove free Gd^{3+} as a precipitate of $Gd(OH)_3$. The precipitate was removed by filtration and obtained crude mixture was purified by a reversed phase HPLC (column: Shiseido Capcell Pak C18 column (Φ30 x 250 mm), eluent: a gradient of CH_3CN-H_2O (10:90 to 90:10) over 40 min in the presence of 0.1% TFA). After the purity of obtained fraction was confirmed by an analytical HPLC (Figure S25) and the collected fraction was dried under vacuum to provide a colorless solid **S11** (0.072 g, 0.08 mmol, Y = 40%); IR (cm^{-1}): 3282 (O–H), 3098 (N–H), 2980 (C–H), 2938 (C–H), 2877 (C–H), 1733 (C=O), 1625 (C=O), 1368, 1318, 1271, 1144, 1085, 1002, 934, 799, 717; HRMS (ESI^+) *m/z*: $[M+H]^+$ calcd for $C_{32}H_{56}Gd_1N_8O_{12}^+$, 902.3261; found, 902.3262.

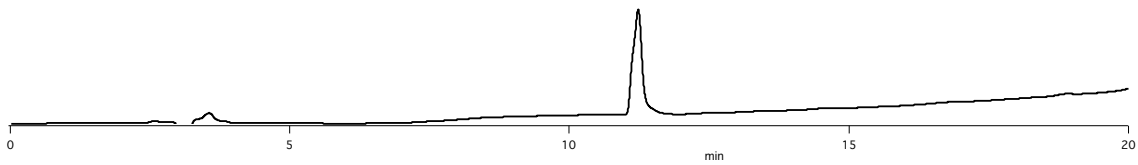

Figure S25. Analytical HPLC diagram of the purified compound **S11** (column: Shiseido Capcell Pak C18 column (Φ 4.6 mm x 250 mm), eluent: a gradient solvent system of CH_3CN-H_2O (10:90 to 98:2, over 20 min) in the presence of 0.1% TFA, flow rate: 1 mL/min, and detection: 220 nm).

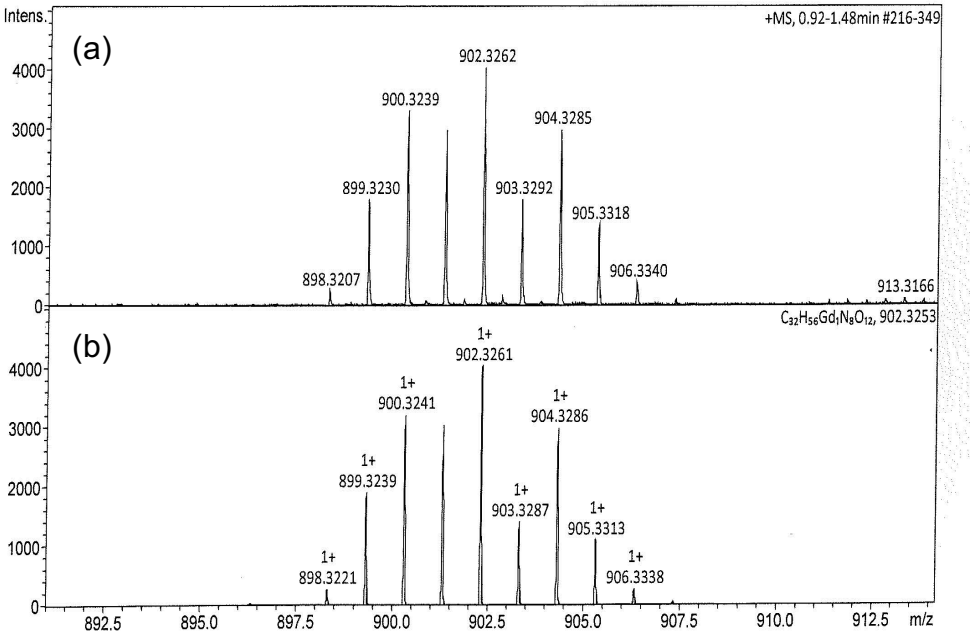

Figure S26. HR-ESI MS spectrum of **S11** (measured (a) and simulated (b)).

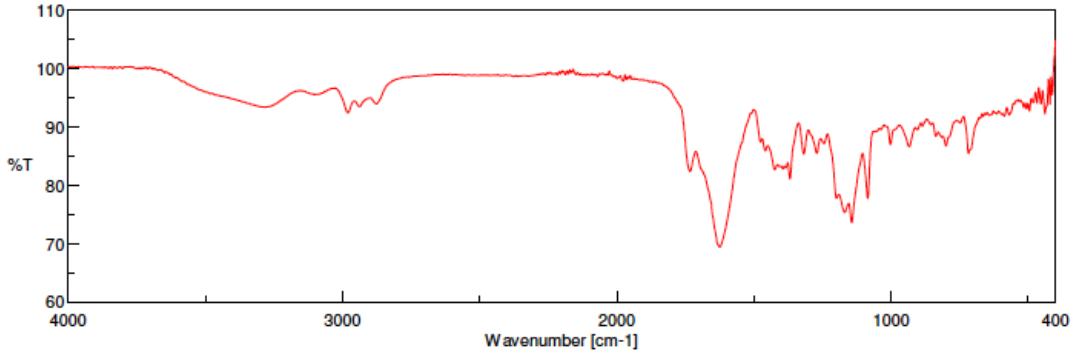

Figure S27. FT-IR ATR spectrum of **S11**.

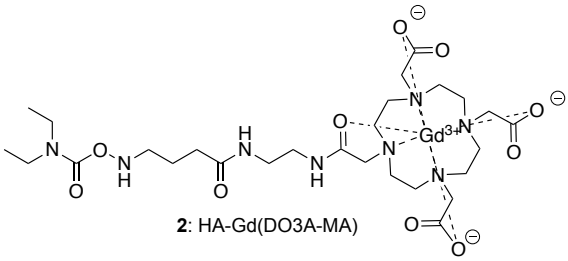

HA-Gd(DO3A-MA) (2). To a suspension of **S11** (5 mg, 6.2 μmol, 1 equiv) in CH_2Cl_2 (0.5 mL), TFA (0.5 mL) was added. The reaction mixture was stirred at room temperature for 15 min to see the completion of reaction monitored by LC-MS (Figure S28b). The solvents were removed by N_2 flow to obtain colorless solids **2**; IR (cm^{-1}): 32723 (O–H), 3098 (N–H), 2875 (C–H), 2360 (C–H), 1749 (C=O), 1621 (C=O), 1406, 1317, 1269.9, 1132, 1082, 1001, 936, 903, 797, 705; HRMS: (MALDI$^+$) *m/z*: $[M+H]^+$ calcd for $C_{27}H_{48}Gd_1N_8O_{10}^+$, 802.2729, found: 802.2757.

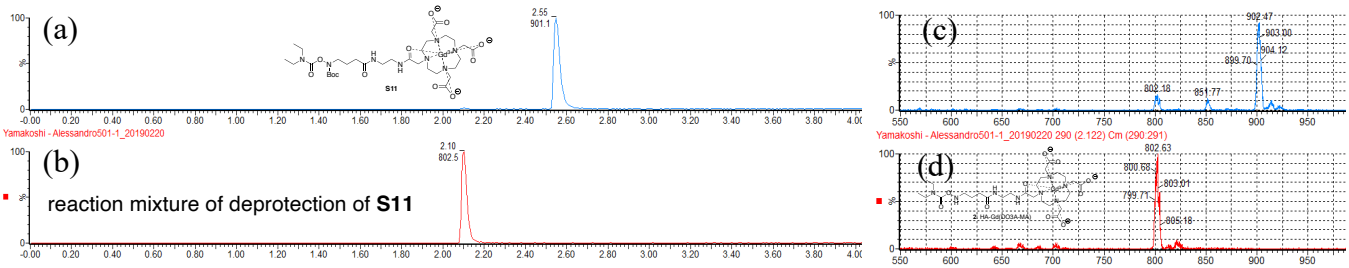

Figure S28. Reaction process of *N*-Boc deprotection of **S11** to HA-Gd(DO3A-MA) **2** monitored by LC-MS Ion chromatogram (*m/z* 750-950) of **S11** (a) and the reaction mixture (15 min) (b) with ESI-MS spectra correspomding to the main peak (c-d). LC-MS detector: Micromass Autospec Ultima-EI-Sector-MS LC-MS system, column: Aquity UPLC BEH C18 (1.7 µm, Φ 2.1 mm x 50 mm), elution: CH_3CN in water (2-98% in 4 min) with 0.1% (v/v) HCOOH, flow rate: 1.0 mL/min.

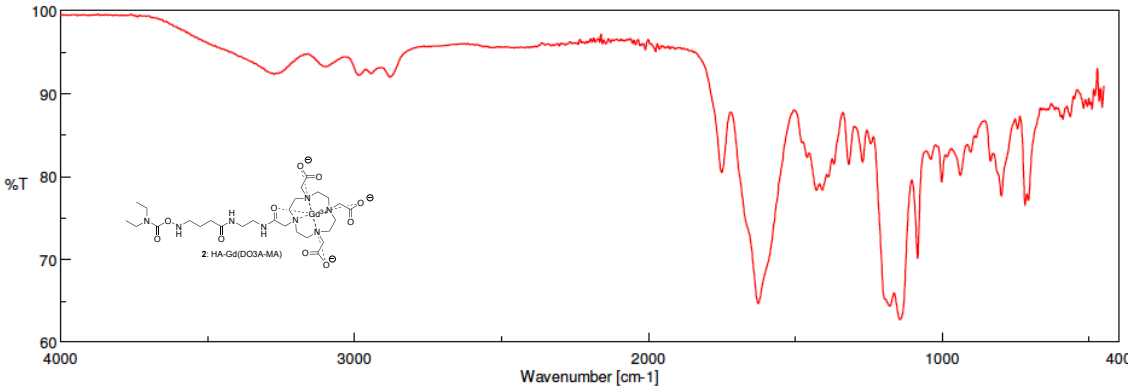

Figure S29. FT-IR ATR spectrum of compound **2.**

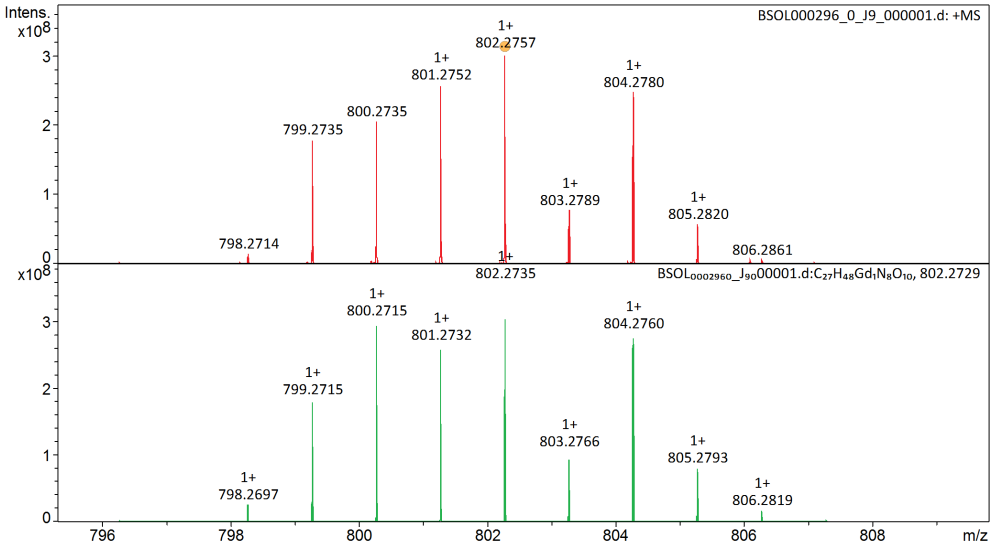

Figure S30. HR-MALDI-MS of **2** (top) with simulation (bottom).

2. Preparation of PGd-LNP nanoparticle

2.1 Preparation of lipid nanoparticle with KAT moieties (LNP-KAT)

The lipid nanoparticle with OA-KAT (**LNP-KAT**) was prepared according to our previous report as below.[1] To a solution of a mixture of three lipid substances – phosphatidylcholine from egg (PC, 33.8 mg, 45 μmol, Tokyo Chemical Industry, Co. LTD., Tokyo, Japan), triolein (TO, 29.2 mg, 33 μmol, Acros) and cholesteryl oleate (CO, 9.4 mg, 17 μmol, Alfa Aesar) –, in a ratio of PC-TO-CO (45:33:17, mol/mol/mol) in a mixture of $CHCl_3$-MeOH-acetone (2:1:1, v/v/v) (90 mL), the KAT derivative of oleic acid[1] (**OA-KAT**, 1.9 mg, 5 μmol, 5 mol% of total lipid) in MeOH-acetone (1:1, v/v) (30 mL) was added and thoroughly mixed in a round bottom flask. The solvents were slowly removed by rotary evaporator to make a thin lipid film on the bottom of the flask, which was further lyophilized overnight to remove all trace of organic solvents. To this dried thin film, 4 mL of Tris-HCl buffer (10 mM, pH 8.0, containing KF (10 mM) and BHT (1 mg L^{-1})) was added, mixed with a vortex mixer for 1 min, and treated under sonication in ice bath for 2 h using an EMMI® 40HC sonicator (EMAG-AG, Mörfelden-Walldorf, Germany). The obtained suspension of lipid mixture was extruded by a Lipex 10 mL extruder (Lipex Biomembranes, Burnaby, BC, Canada) for 10 times at 50 °C using two stacked polycarbonate membrane filters (pore sizes: 0.05 μm and 0.1 μm). The obtained nanoparticle dispersion was filtered through a filter (0.45 μm, Chromafil® Xtra PTEF-45/25, Macherey Nagel GmbH & Co. KG, Düren, Germany), washed three times with Tris-HCl buffer (10mM, pH 8.0, containing KF (10 mM) and BHT (1 mf L^{-1})) by spin filtering (Amicon centrifuge filter 50 kDa cutoff, Merck KGaA) to remove the free un-bound lipids, which were not incorporated into the particle. The filtrate (**LNP-KAT** (5%) particle) was kept in Tris-HCl buffer (10 mM, pH 8.0, containing KF (10 mM) and BHT (1 mg L^{-1})) at 4 ºC before being subjected to the surface functionalization. Similarly, **LNP-KAT** (10%) particle suspension (4 mL) was prepared with the same preparation protocol described above, using a lipid mixture of PC (30.1, 40 μmol), TO (29.2, 33 μmol), CO (9.4 mg, 17 μmol) and **OA-KAT** (3.8, 10 μmol).

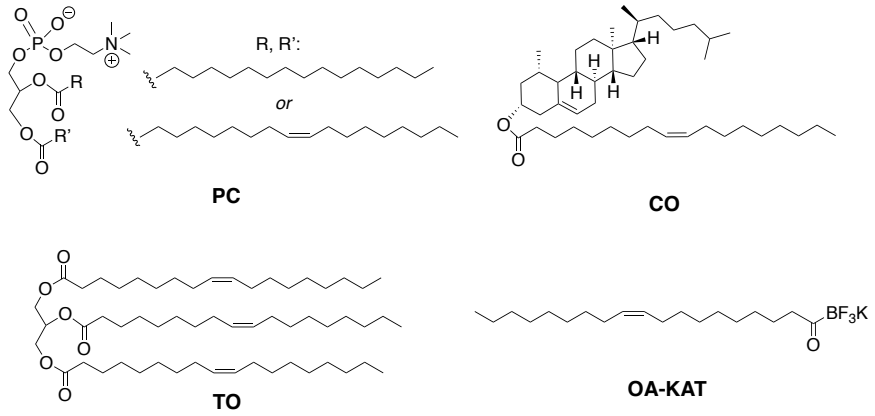

Figure S31. Structures of lipid materials used in the formation of LNP-KAT.

2.2 Preparation of LNP particles (*on-surface* KAT ligation of LNP-KAT with hydroxylamine derivatives 1, 2, and 3)

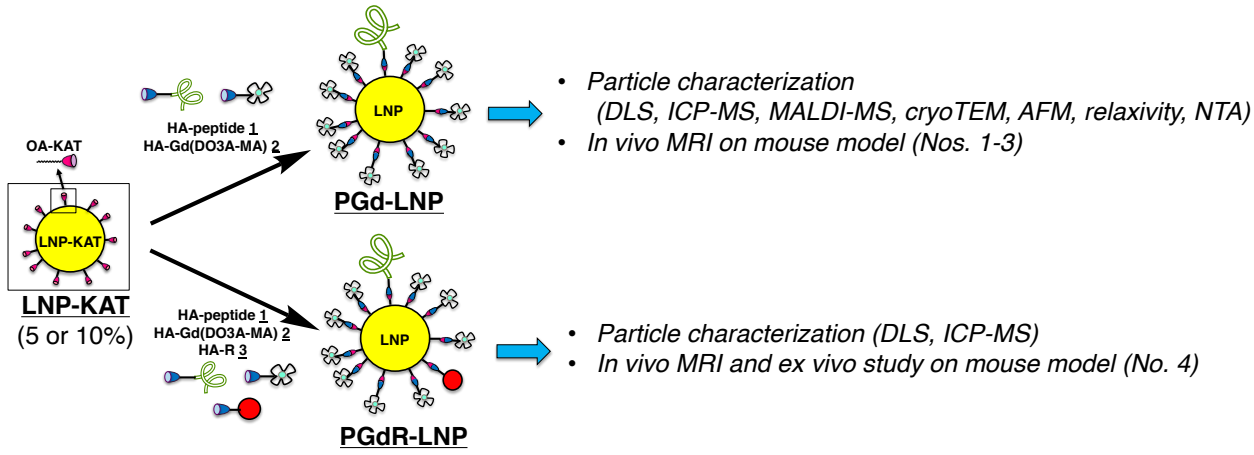

Figure S32. Schematic illustration of the functionalized LNPs by KAT ligation.

Preparation of PGd-LNP particle from LNP-KAT 5%. To a mixture of 10 mM KF in phosphate buffer (10 mM, pH 5.8, 32 mL) and 0.1 M HCl (400 µL), a solution of HA-peptide (**HA-P**) **1** (0.48 µmol) in H_2O (200 µL) and a solution of HA-Gd(DO3A-MA) (**HA-Gd**) **2** (4.32 µmol) in H_2O (700 µL) were added. Subsequently, **LNP-KAT** (5%) particle (with estimated KAT content of 4.1 µmol by ICP-MS analysis of B, please see section 2.3.1) in 8 mL of Tris-HCl buffer (10 mM, pH 8.0, 2-batchs prepared in section 2.1) was added. The pH of the reaction mixture was measured to be 5.2. The reaction was stirred overnight at room temperature. The crude mixture was concentrated to a volume of 1.5 mL by spin filtering (Amicon centrifuge filter 50 kDa cutoff) and washed with 5 mL of PBS (-) (pH 7.4) for three times to remove the unreacted **1** and **2**. The obtained nanoparticle was reconstituted to 8 mL in PBS (-) (pH 7.4) for the characterization.

Preparation of PGd-LNP particle from LNP-KAT 10%. To a mixture of 10 mM KF in phosphate buffer (10 mM, pH 5.8, 36 mL) and 0.1 M HCl (400 µL), a solution of **HA-P 1** (0.48 µmol) in H_2O (200 µL) and a solution of **HA-Gd 2** (4.32 µmol) (mol ratio of HA detivatives are in H_2O (700 µL) were added. Subsequently, **LNP-KAT** (10%) particle (with estimated KAT content of 4.8 µmol by ICP-MS analysis of B, please see section 2.3.1) in 4 mL of Tris-HCl buffer (10 mM, pH 8.0, 1-batch prepared in section 2.1) was added. The pH of the reaction mixture was measured to be 5.2. The reaction was stirred overnight at room temperature. The crude mixture was concentrated to a volume of 0.5 mL by spin filtering (Amicon centrifuge filter 50 kDa cutoff) and washed with 2.0 mL of PBS (-) (pH 7.4) for three times to remove the unreacted **1** and **2**. The obtained nanoparticle was reconstituted to 8 mL in PBS (-) (pH 7.4) for the characterization.

Preparation of PGdR-LNP particle from LNP-KAT 10%. The **PGdR-LNP** particle was prepared in a similar manner as **PGd-LNP**, using **LNP-KAT** (10%) particle as a starting material. To an aqueous solution of a mixture of **HA-P 1** (0.48 μmol), **HA-Gd 2** (4.08 μmol), HA-sulforhodamine B (**HA-R**) **3** (0.24 μmol) in a mole ratio of 10:85:5 in a mixture of pH 5.8 phosphate buffer 36 mL (10 mM, containing 10 mM of KF) and 0.1 M HCl 200 μL, a dispersion of **LNP-KAT** (10%) (4 mL in Tris-HCl buffer (10 mM, pH 8.0) was added.

2.3 Characterization of particles

2.3.1 ICP-MS for B and Gd contents in LNP-KAT and PGd-LNP particles

The ICP-MS or ICP-OES analyses of B and Gd contents were measured on an Element XR sector-field inductively coupled plasma mass spectrometer (Thermo Fisher Scientific, Waltham, MA, USA) or a Horiba Ultra 2 inductively coupled plasma-optical emission spectrometer (Horiba Ltd., Kyoto, Japan). An aliquot (100 μL for B analysis and 20 μL for Gd analysis) of each particle dispersion was dried on a hot plate and digested by refluxing in conc. HNO_3 (1 mL) for 16 hours. Subsequently, each sample was dried again and dissolved in 1.0 mL of 2% HNO_3 (v/v) (0.3 M) before being subjected to the ICP-MS or ICP-OES analyses. Calibration curves were prepared using standard solutions of B and Gd (Alfa Aesar B ICP standard and Gd ICP standard (Thermo Fisher (Kandel) GmbH, Kandel, Germany) in a concentration range of 5-200 μM. In case of ICP-MS measurements, samples were introduced into the mass spectrometer via a PFA nebulizer with an uptake rate of 50 $\mu L \cdot min^{-1}$ attached to a cyclonic glass spray chamber. In general, in this laboratory, long-term accuracy and precision are assessed using two secondary multielement standards: National Research Council of Canada river standard SLRS-5 (now replaced by SLRS-6) and USGS shale standard SGR1. The concentrations obtained matched certified values to within 5-10% (2SD) for most of the elements of interest. In this laboratory, boron is not routinely measured, therefore no long-term data are available. However, the accuracy and precision within the analytical session were determined by repeated analysis of SRM NIST 1640 and were determined to be with 10 and 17% (2SD), respectively.

Table S1. Quantification of B in **LNP-KAT (5%)** and amount of incorporated **OA-KAT**

run	initially added **OA-KAT** [μM]	B contents in **LNP-KAT (5%)** [μM]*	incorporation yield of **OA-KAT** in **LNP-KAT** [%]
1	1250	513.0	41.0
2	1250	514.8	41.2
average		514	41

*Estimated by ICP-MS.

Table S2. Quantification of B and Gd of **PGd-LNP** by ICP-MS analysis

run	B contents of f **PGd-LNP** [μM]*	consumed B [μM]**	% of consumed B [%]	Gd contents of **PGd-LNP** [μM]*	yield of Gd addition relative to the total B of **LNP-KAT** [%]***	yield of Gd addition relative to consumed B [%]	yield of Gd addition relative to consumed B [%]***
1	197.6	316.4	61.6	206.5	44.6	65.3	72.5
2	212.8	301.2	58.6	227.4	49.2	75.5	83.9
3	272.0	242.0	47.1	216.7	46.8	89.5	99.5
average	227.5±19.7	286.5±19.7	55.8±3.82	216.9±5.23	46.9±1.01	76.8±6.10	85.3±6.77

*Determined by ICP-MS analysis. **Estimated relative to the total B contents of **LNP-KAT 5%** (514 μM, see table S1). ***Taking into account the portion of HA-peptide (10% of total HA reagents).

2.3.2 MALDI-MS analysis of PGd-LNP particle

The MALDI of the **PGd-LNP** was recorded on a Bruker SolariX-FTICR 9.4 T MS (Bruker Daltonics). An aliquot (50 μL) of the particle diepersion of **PGd-LNP** in PBS (pH 7.4) was dried by N_2 flow and reconstituted in 200 μL of a mixture of H_2O and CH_3CN (1:1, v/v). The mixture was then further diluted 10 times with a saturated solution of α-cyano-4-hydroxycinammic acid (HCCA) in a mixture of H_2O and CH_3CN (1:1, v/v) before the MALDI analysis.

2.3.3 DLS analyses

DLS measurements were performed on a Malvern Nano-ZetaSizer (Malvern Instruments Ltd., Worcestershire, UK), equipped with a 5 mW HeNe laser (wavelength: 632.8 nm) and a digital logarithmic correlator. The normalized intensity autocorrelation functions were measured at an angle of 173°. An aliquot (20 μL) of each obtained particle was diluted with Tris-HCl buffer (10 mM, pH 8.0) or PBS (-) (pH 7.4) to 0.8 – 1 mL for the measurements, which were carried out at 25 ºC.

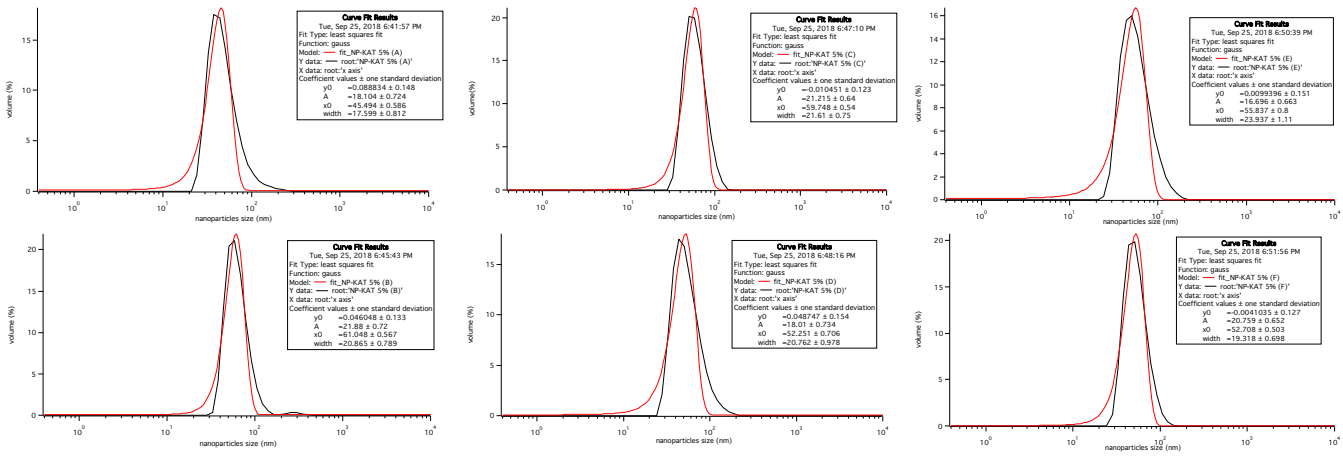

Figure S33. DLS of **LNP-KAT (5%)** in 10 mM Tris-HCl buffer (10 mM KF) pH 8.0 with 6 different lots.

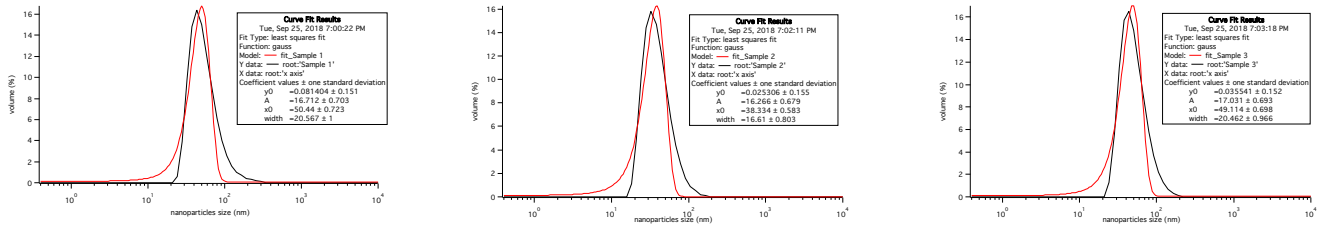

Figure S34. DLS of **PGd-LNP** in PBS (-) (pH 7.4) with 3 different lots.

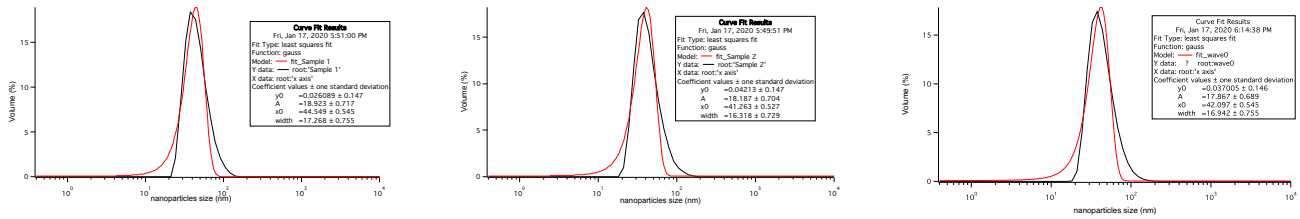

Figure S35. DLS of **PGdR-LNP** in PBS (-) (pH 7.4) with 3 different lots.

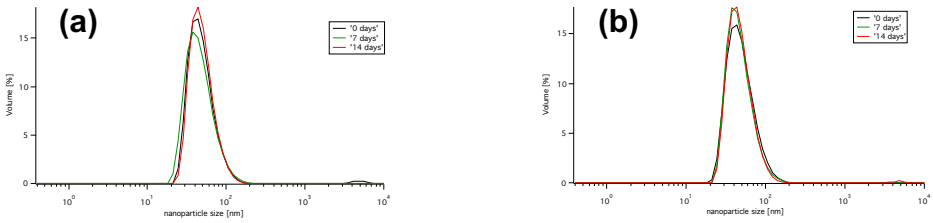

Figure S36. Stability test of **LNP-KAT** and **PGd-LNP** after 0, 7 and 14 days of storage at 4 °C by DLS. (a) **LNP-KAT** in 10 mM Tris-HCl buffer (10 mM KF) pH 8.0. (b) **PGd-LNP** in PBS (-) pH 7.4.

2.3.4 AFM measurements

Samples were prepared based on some previously reported procedures for NP imaging[4] with modifications. Mica (Ted Pella Inc., Redding, CA, USA) was freshly cleaved with a scotch-tape to reveal a fresh layer devoid of organic contaminants. An aliquot (10 µL) of each nanoparticle suspension, which was diluted 5 times with PBS (pH 7.4), was deposited onto the mica surface and left for 10 min for immobilization. Subsequently, 10% formalin solution (10 µL) was added and left additionally for 10 min. The substrate was washed with PBS (50 µL) to remove excess nanoparticles, and added with an additional aliquot (50 µL) of PBS, and kept for 30 min prior to AFM imaging. AFM imaging was performed on a Bruker Dimension Icon AFM (Bruker) in Peak Force Tapping mode in liquid with an SNL 10-A cantilever (Bruker, deflection sensitivity: 30 nm/V, spring constant: 0.35 N/m, frequency: 80 KHz). The engage setpoint was set to 0.05 V with initial imaging force at roughly 50-80 pN to make

[4] Zaske, A. M.; Danila, D.; Queen, M. C.; Golunski, E.; Conyers, J. L., Biological Atomic Force Microscopy for Imaging Gold-Labeled Liposomes on Human Coronary Artery Endothelial Cells. *J Pharmaceutics* **2013**.

engage settings rather soft so that the tip underwent minimum impact when approaching the surface. Imaging was performed using a peak force frequency of 2 kHz, and peak force amplitude of 10 nm. Images were acquired at line rate of 1-1.2 Hz with 512 pixels per line. Data were analyzed using the Bruker Nanoscope Analysis (Bruker AXS, CA, USA) for line-by-line flattening and removal of tilt using first order polynomial.

2.3.5 CryoTEM imaging

The microscopical characterization of the particles in their hydrated state was carried out on a Tecnai F20 cryoTEM (FEI/Thermo Fisher Scientific). The 300-mesh lacey carbon-coated copper grids (Quantifoil Micro Tools GmbH, Jena, Germany) were glow discharged using an Emitech K100X (Quorum Technologies Ltd., Laughton, GB) for 30 sec. An aliquot of particle suspension (3 µL) was applied onto the grids in a Vitrobot Mark II (FEI/Thermo Fisher Scientific) and the excess of the particles was removed by controlled blotting. A mixture of liquid ethane/propane was used for sample vitrification. The grids were then transferred on a Gatan cryo-transfer holder (Gatan, Inc., Pleasanton, CA, USA) into the microscope and kept at –180 °C during observation. Micrographs were recorded under low dose conditions (<500 e^{-}/nm^{2}) using a Falcon II 4K Camera (FEI Thermo Fisher Scientific), operating the microscope at 200 kV acceleration voltage in bright field mode.

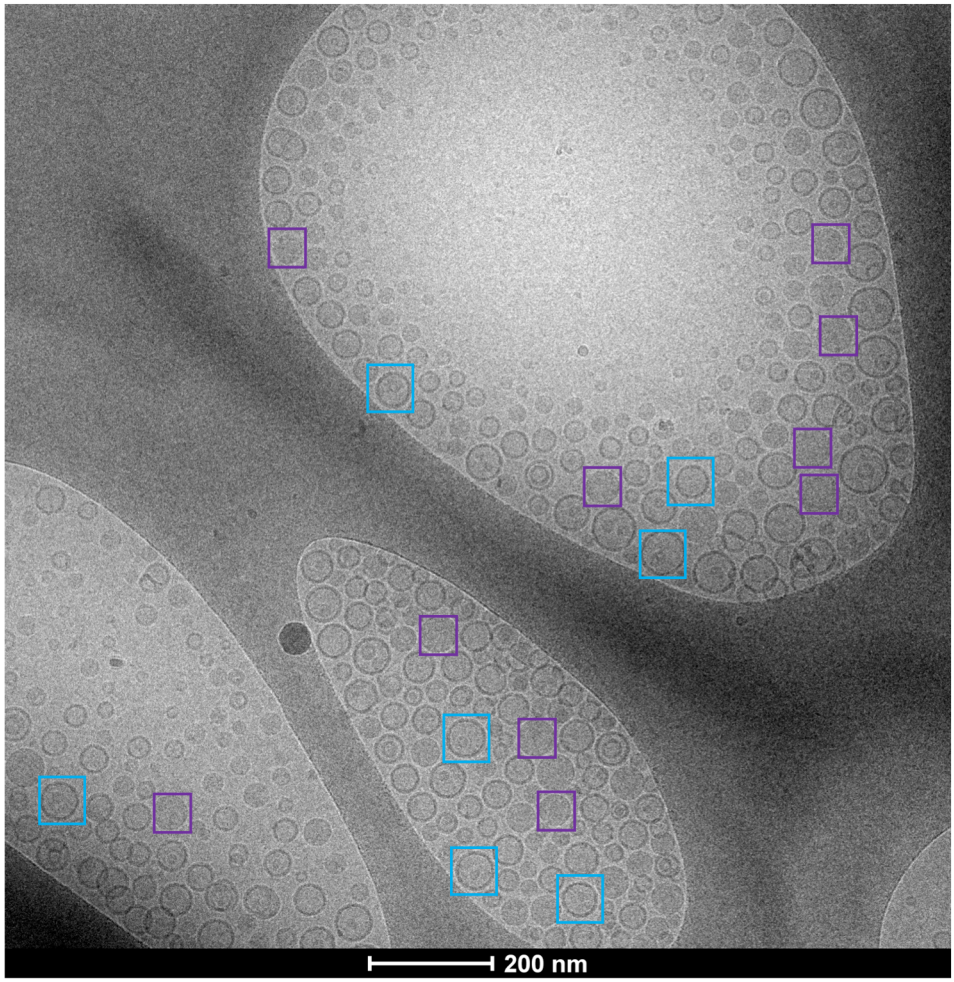

Figure S37. Expanded cryoTEM image of **LNP-KAT (10%)** revealing two types of NPs with lipid monolayer (□) and bilayers (□). Representative particles are marked.

2.3.6 NTA measurements[5]

The number of LNP in 1 mL of **PGd-LNP** dispersion was determined by a nanoparticle tracking analysis (NTA) using Zetaview® (Particle Metrix, Meerbusch, Germany). The sample (2 mL) was injected into the sample cell. Subsequently, the particles were illuminated with a 405-nm laser sheet (45 mW) and imaged with a video camera mounted on a 10× microscope objective oriented 90° to the laser sheet. The camera took the images in 11 defferent positions in the sample cell, probing 0.4 nL of volume at each position. The aspect ratio of the camera is 640 pixels × 480 pixels, with an effective pixel size of 0.7 µm/pixel. Before the NTA measurements of the LNP, a reference stock solution of polystirene provided by the

[5] Defante, A. P.; Vreeland, W. N.; Benkstein, K. D.; Ripple, D. C. Using Image Attributes to Assure Accurate Particles Size and Count Using Nanoparticles Tracking Analysis. *J. Pharm. Sci.*, **2018**, *107*, 1383-1391.

manufacturer was used to optimize the camera settings for alignment and focus. The provided reference was diluted to particle count of 6.0×10^7 particles/mL as recommended by the manufacturer.

Table S3. Estimation of Gd numbers per **PGd-LNP** particle by NTA in combination with ICP-MS data

Samples		numbers of LNP per 1 mL*	Gd contents in **PGd-LNP** dispersion [μM]**	number of Gd per 1mL of **PGd-LNP**	number of Gd per **PGd-LNP**
PGd-LNP 5%* **	1	4.8×10^{13}	206.5	1.24×10^{17}	2583
	2	4.1×10^{13}	227.4	1.37×10^{17}	3341
	3	5.0×10^{13}	216.7	1.30×10^{17}	2600
average		$4.6 \pm 0.26 \times 10^{13}$	216.9±5.2	$1.30 \pm 0.03 \times 10^{17}$	2841±216
PGd-LNP 10%** **	1	4.5×10^{13}	372.8	2.24×10^{17}	4978
	2	5.6×10^{13}	390.2	2.35×10^{17}	4196
	3	4.6×10^{13}	361.3	2.18×10^{17}	4739
average		$4.9 \pm 0.32 \times 10^{13}$	374.8 ±7.3	$2.26 \pm 0.04 \times 10^{17}$	4638±200

* NTA data. ** ICP-MS data. ***Prepared from **LNP-KAT 5%**, ****Prepared from **LNP-KAT 10%**.

2.3.7 Relaxivity measurements

The Proton relaxivities at 60 MHz were measured on a Bruker WP80 NMR electromagnet adapted to variable field measurements and controlled by a Stelar SMARTracer PC-NMR console (Stelar s.r.l., Pavia, Italy). The temperature was monitored by a VTC91 temperature control unit and maintained by a gas flow. The temperature was determined by previous calibration with a Pt resistance temperature probe. Relaxivities at 400 MHz were measured on a Bruker AVANCE NMR spectrometer. The temperature was calculated according to previous calibration with ethylene glycol and methanol. The Gd concentration of the sample was 193 μM.

2.3.8 Determination of surface reaction yield in the synthesis of PGdR-LNP

The quantitative analysis for the determination of the amount of sulforhodamine B attached to the **PGdR-LNP** was performed by UV-vis spectroscopy using a Varian Cary 500 UV-vis spectrophotometer. Five solutions of compound **3** were prepared in a mixture of MeOH-PBS 9-1 at the concentration of 2, 3, 4, 5, 6 μM and used as standard solutions. The calibration curve was obtained by plotting the maximum absorbance (565 nm) *vs* the concentration of the standard solutions (Figure S38).

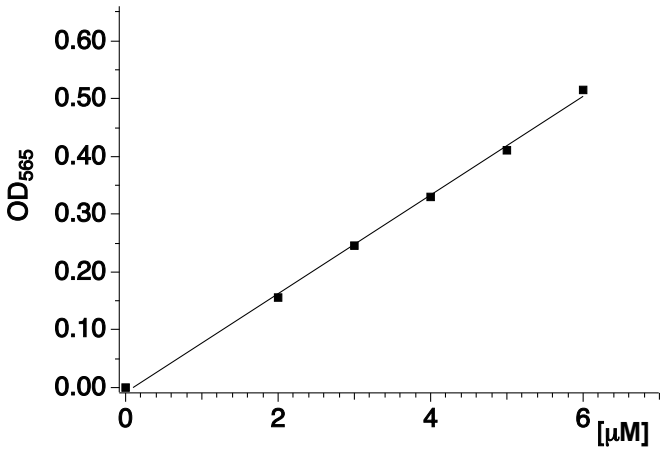

Figure S38. Calibration with HA-sulforhodamine B **3** by OD_{565}.

Table S4. Surface reaction efficiency in the formation of **PGdR-LNP** from **NP-KAT 10%**

samples	OD_{565}	conc. of rhodamine B [μM]*	yield of rhodamine B addition [%]**	conc. of Gd^{3+} [μM]***	yield of Gd^{3+} addition [%]**	yield addition of rhodamine and Gd^{3+} [%]**	estimated surface reaction [%]****
1	0.37	44.4	3.7	449.0	37.4	41.1	45.7
2	0.28	34.0	2.8	382.8	31.9	34.7	38.6
3	0.29	35.3	2.9	391.8	32.7	35.6	39.5
average		37.9±2.8	3.16±0.24	407.9±18.0	34.0±1.50	37.1±1.73	41.3±1.92

*Obtained with the calibration in Figure S38. **Calculated from the total B contents in **LNP-KAT 10%** (1200 μM, by ICP-MS). ***Obtained by ICP-MS analysis of the samples. ****Calculated from total B contents of **LNP-KAT** by taking into account of addition of HA-peptide (10% of total HA reagents). **HA-P 1**, **HA-Gd 2**, and **HA-R 3** were added in a mol ratio of 10:85:5 in total of 1.2 equiv to the **OA-KAT** in **LNP-KAT**.

3. *In vivo* MRI and *ex vivo* analyses

3.1 *In vivo* MRI on *apoE*$^{-/-}$ mice and *ex vivo* anaylsis of aorta by ICP-MS

Atherosclerotic mouse model and *in vivo* injection. All the animal procedures were approved by the Institutional Animal Care and Use Committee (IACUC) of the University of Pennsylvania. The male *apoE*$^{-/-}$ mice were purchased from the Jackson Laboratory. The mice started receiving HFD (42% kcal from fat, Teklad#88137) at 8 weeks of age and the HFD was continued for two months. Prior to injection, the **PGd-LNP** sample was concentrated in filter tubes (50 kDa) by centrifugation (1000 rcf at 4 °C) to a suitable volume (0.25 mL) for the injection to a mouse. No aggregation was observed after the centrifugation. Under anesthesia, the **PGd-LNP** particle was injected *via* a catheter placed in the tail vein of the mouse.

***In vivo* MRI test.** All MRI was performed on a 9.4 T horizontal bore MR spectrometer (DirectDrive®, Agilent, Palo Alto, CA) equipped with a 12-cm (ID) gradient coil. The mouse was positioned prone in a quadrature volume radio frequency (RF) coil (ID = 3.5 cm, length = 8 cm, m2m imaging/Polarean) tuned to ^{1}H resonance frequency (400 MHz). During imaging, the mouse was sedated with 0.8−1% of isoflurane mixed with air (flow rate = 1 L/min). ECG, respiration and core temperature of the mouse were monitored by an MRI-compatible vital sign monitoring system (SA Inc, Long Island, New York). The rectal temperature was maintained at 37 ±0.2 °C by a feedback loop that turns on/off warm air directed into the magnet bore. Scout images were acquired to capture the aortic arch with three rising branches (LC, LS and BA). Then the image plane was placed to cut through the three aortic branching points. This image plane was used to acquire the "White Blood" (WB), where the blood signal in the lumen of aorta is not suppressed, as well as "Black Blood" (BB) images, where the blood signal is suppressed (thus black). To obtain WB image, ECG-gated multi-slice gradient echo sequence (TR = 1 heartbeat, about 120 ms, TE = 2.4 ms) was employed with FOV = 26 x 25 mm, matrix size = 192 x 128, slice thickness = 0.8 mm. To obtain BB images, ECG-gated multi-slice FLASH (Fast imaging with Low Angle Shot) (TR = 76 ms, TE =0.97 ms, FA=40 degree) was applied to the same slice. Due to the long interval between MRI sessions, we relied on the unique anatomy of the aortic arch, its branching points, and other thoracic arteries in the imaging plane for the comparison of pre- and post-injection images. For images acquired after **PGd-LNP** injection, BB was further combined with fat suppression option in the MRI protocol although such option is not necessary to detect enhancement.

***Ex vivo* analysis of aorta by ICP-MS.** The mice were euthanized 48 h after the injection of **PGd-LNP**. To obtain the clean aorta from the *apoE*$^{-/-}$mice, PBS buffer pH 7.4 was perfused in the blood stream from the left ventricle of the heart and the right atrium was gently cut in order to absorb the perfusion liquid by sterile gauzes. The aorta was then dissected utilizing a dissecting microscope and the aortic arch

was collected. Under a dissection microscope, the presence of atherosclerotic plaques was clearly visible. The ICP-MS analysis of the Gd contents in the mice aorta (ng of Gd^{3+} per mg of dry tissue) was carried out in Pennsylvania Animal Diagnostic Laboratory System in New Bolton Center (Kennett Square, PA, USA).

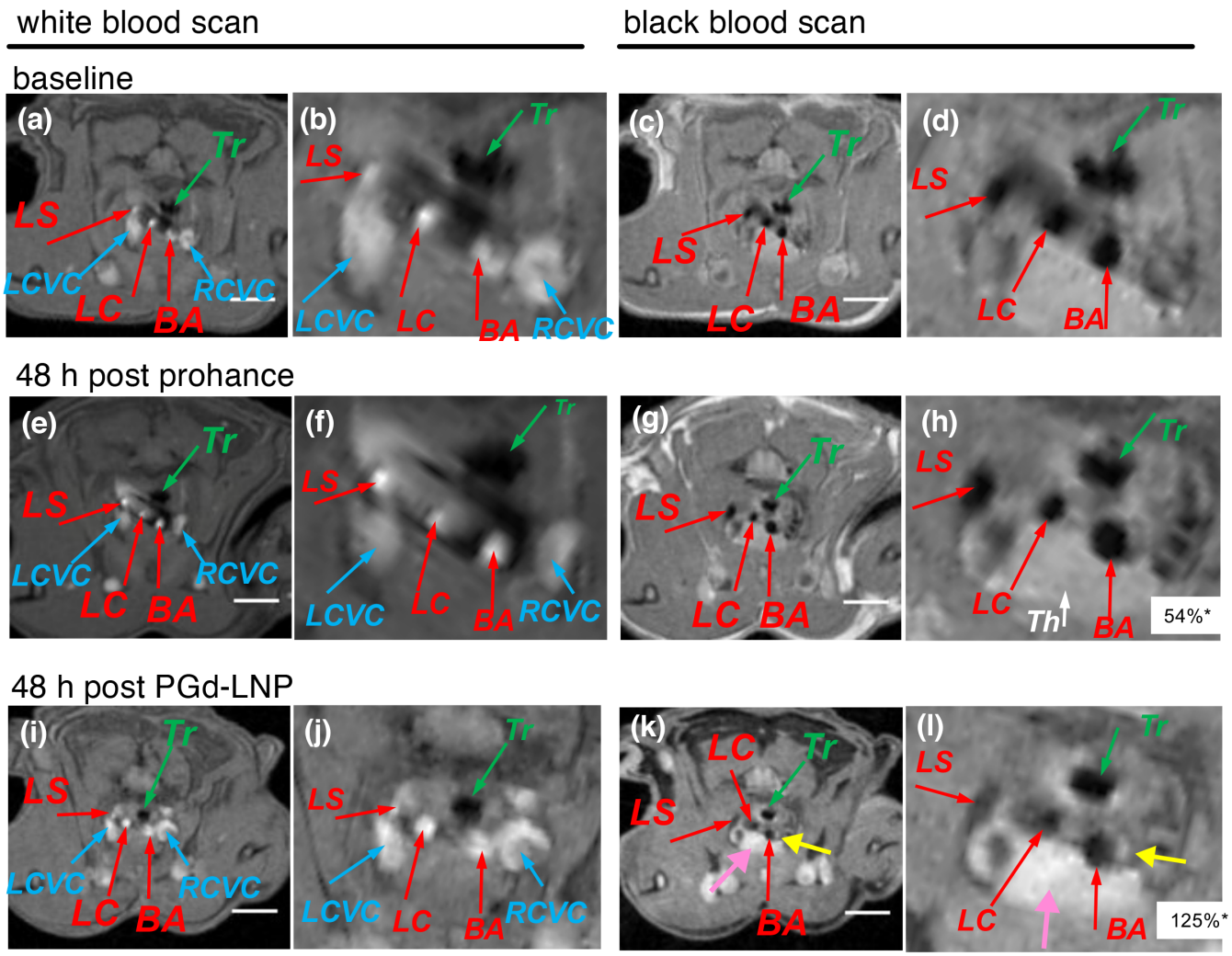

Figure S39. *In vivo* MR images of an atheroma in the artery of an *apoE*$^{-/-}$ mouse (No. 1) taken pre-injection (a-d), 48 h post-injection of ProHance® (e-h), and 48 h post-injection of **PGd-LNP** particle (i-l) with white blood images (a, b, e, f, i, j) and black blood images (c, d, g, h, k, l). The three branches of the aortic arch were identified by red arrows: BA = brachiocephalic artery; LC = left carotid artery; LS = left subclavian artery. The left cranial vena cava (LCVC) and right cranial vena cava (RCVC) are identified by blue arrows. The trachea is identified by green arrows. Yellow arrows point to enhancement of atherosclerotic plaque in the BA wall. Pink arrows point out enhancement of thymus. *The normalized signal enhancement (%NSE) calculated as shown in section 3.3. White bars correspond to 5-mm.

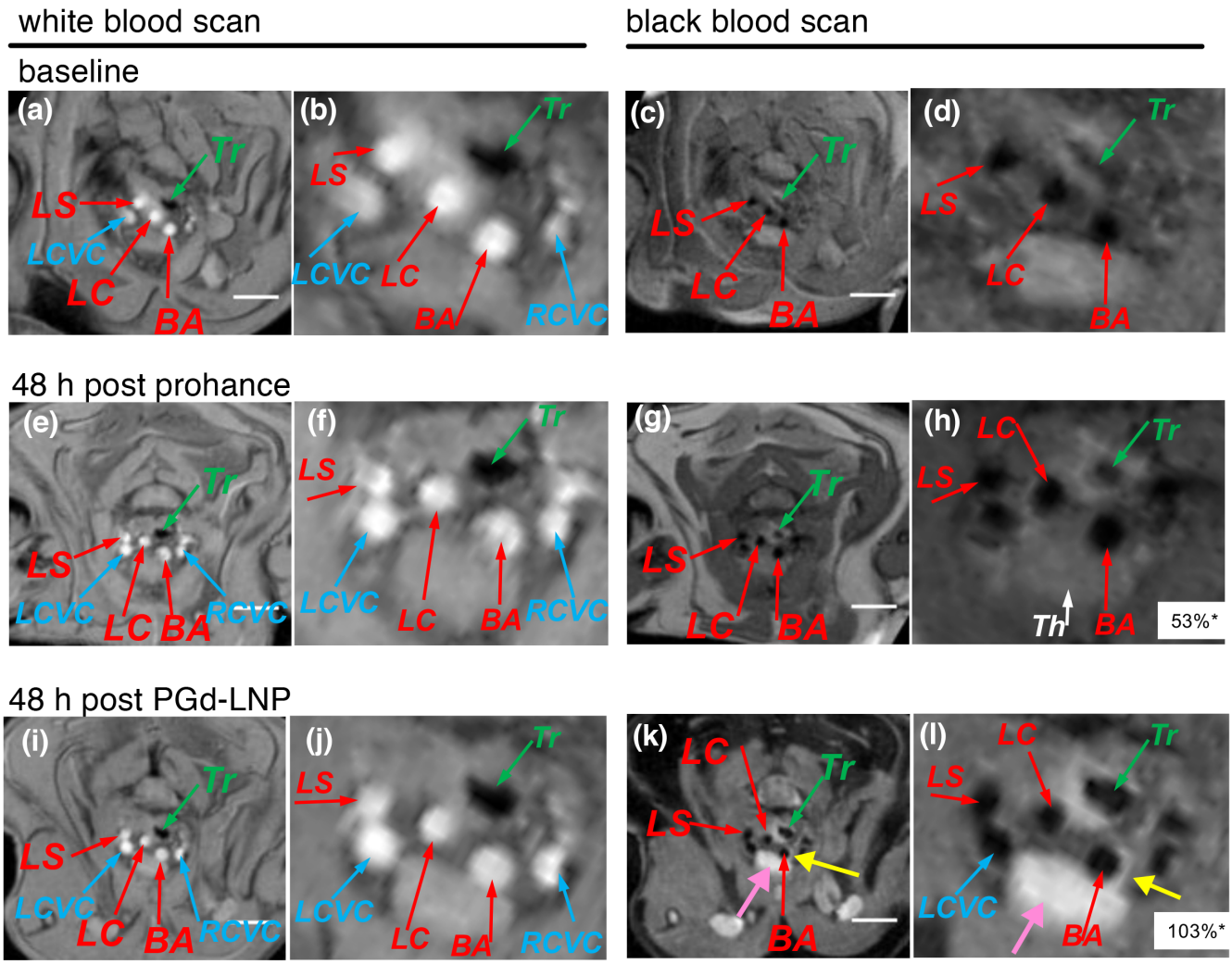

Figure S40. *In vivo* MR images of an atheroma in the artery of an *apoE*$^{-/-}$ mouse (No. 2) taken pre-injection (a-d), 48 h post-injection of ProHance® (e-h), and 48 h post-injection of **PGd-LNP** particle (i-l) with white blood images (a, b, e, f, i, j) and black blood images (c, d, g, h, k, l). The three branches of the aortic arch were identified by red arrows: BA = brachiocephalic artery; LC = left carotid artery; LS = left subclavian artery. The left cranial vena cava (LCVC) and right cranial vena cava (RCVC) are identified by blue arrows. The trachea is identified by green arrows. Yellow arrows point to enhancement of atherosclerotic plaque in the BA wall. Pink arrows point out enhancement of thymus. *The normalized signal enhancement (%NSE) calculated as shown in section 3.3. White bars correspond to 5-mm.

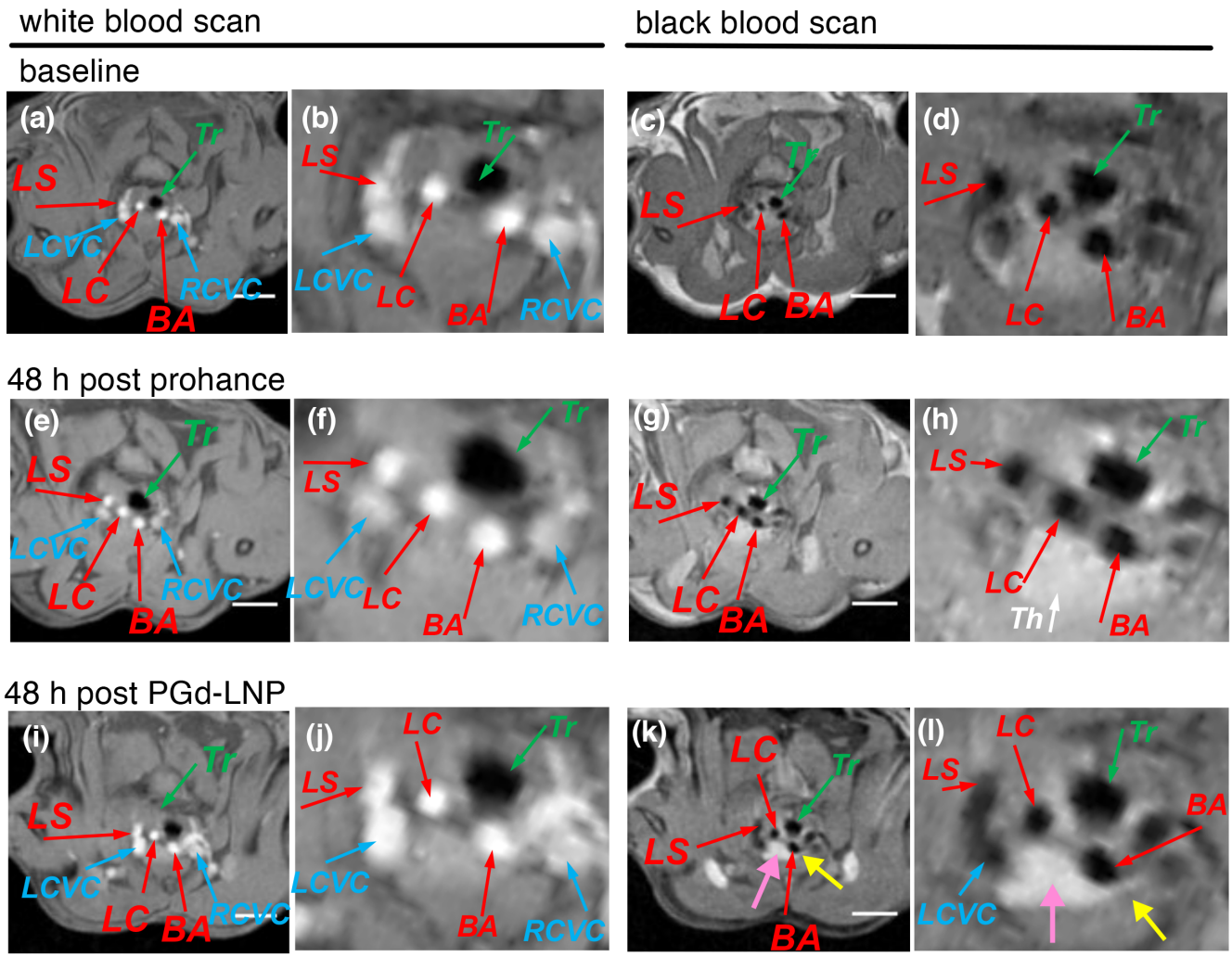

Figure S41. *In vivo* MR images of an atheroma in the artery of an *apoE*$^{-/-}$ mouse (No. 3) taken pre-injection (a-d), 48 h post-injection of ProHance® (e-h), and 48 h post-injection of **PGd-LNP** particle (i-l) with white blood images (a, b, e, f, i, j) and black blood images (c, d, g, h, k, l). The three branches of the aortic arch were identified by red arrows: BA = brachiocephalic artery; LC = left carotid artery; LS = left subclavian artery. The left cranial vena cava (LCVC) and right cranial vena cava (RCVC) are identified by blue arrows. The trachea is identified by green arrows. Yellow arrows point to enhancement of atherosclerotic plaque in the BA wall. Pink arrows point out enhancement of thymus. White bars correspond to 5-mm. The normalized signal enhancement (%NSE) was not obtained due to the overlapping of brachiocephalic artery wall with the enhanced thymus.

3.2 *In vivo* MRI on *apoE*$^{-/-}$ mice and *ex vivo* analyses by cryoViz brighfield and fluorescent imaging

MRI images were taken in a similar manner as described in Section 3.2 above. The same atherosclerotic mouse model used. In order to perform both *in vivo* MRI and *ex vivo* cryoViz analyses, a triply

functionalized **PGdR-LNP** (see section 2.3.8 above) was injected. Since the images taken 24 hours after injection were with higher enhancement compared to the one taken 48 hours after injection, the mouse was subjected to the cryoViz analyses 24 hours after injection.

Immediately after euthanasia by inhalation of carbon dioxide, the mice were covered with Tissue-Tek® Optimal Cutting Temperature (O. C. T.) solution (Sakura Finetek USA, Inc., Torrance, CA, USA). This step ensures that the carcass is wet and no air bubbles are formed in the next step of embedding. The mouse is then embedded in O. C. T. inside an aluminum foil mould. The entire mould is snap-frozen in liquid nitrogen and transferred to BioInVision (Cleveland, OH, USA) for the concomitant cryosectioning and imaging using an automated microtome-blockface episcopic imaging system (CryoViz™, BioInvision) that allows for microscopic, three-dimensional resolution of fluorophores in macroscopic specimens. A 40 µm section thickness was used for whole mouse.[6]

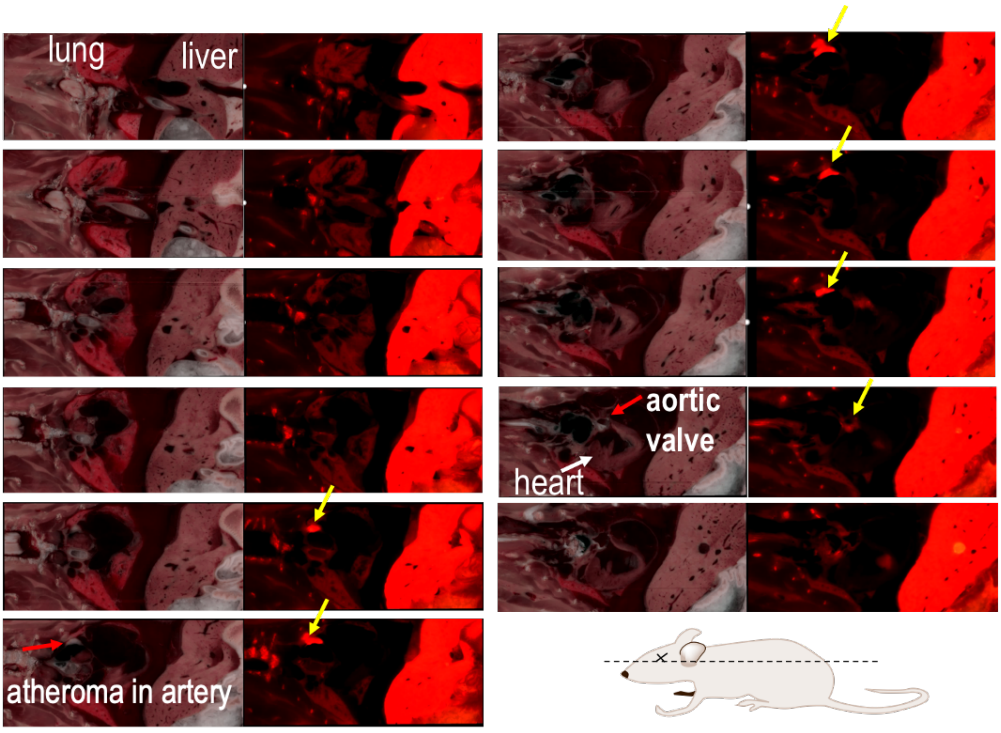

Figure S42. *Ex vivo* cryoViz images of *apoE*$^{-/-}$ (mouse No. 4) injected with **PGdR-LNP**. Sequential coronal view images with brightfield (left) and fluorescence (right) images at the region of interest.

[6] Roy, D.; Breen, M.; Salvado, O.; Heinzel, M.; McKinley, E.; Wilson, D. Imaging System for Creating 3D Block-Face Cryo-Images of Whole Mice. In *Medical Imaging 2006: Physiology, Function, and Structure from Medical Images*; International Society for Optics and Photonics, 2006; Vol. 6143, p 61431E, Wilson, D.; Roy, D.; Steyer, G.; Gargesha, M.; Stone, M.; McKinley, E. Whole Mouse Cryo-Imaging. In *Medical Imaging 2008: Physiology, Function, and Structure from Medical Images*; International Society for Optics and Photonics, 2008; Vol. 6916, p 69161I.

3.3 Determination of the MRI signal enhancement (%NSE)

The normalized signal enhancement (%NSE) was calculated as previously reported,[7] according to the following equation:

$$\%NSE = 100 \times ((I_{wallpost}/I_{musclepost})/(I_{wallpre}/I_{musclepre}) - 1)$$

$I_{wallpre}$ and $I_{wallpost}$ correspond to the signal intensities from the artery wall at pre- and post-injection, respectively. The intensity of the wall (I_{wall}) was calculated by subtracting the signal averaged over the entire artery area defined by the yellow circle (I_{tot}) minus the signal averaged over the artery lumen area defined by the red circle (I_{lum}), normalizing by the area of the artery wall (Figure S43), as shown below:

$$\text{Mean } I_{wall} = [((\text{mean } I_{tot}) \times (A_{tot})) - ((\text{mean } I_{lum}) \times (A_{lum}))]/(A_{tot} - A_{lum})$$

$I_{musclepre}$ and $I_{musclepost}$ are defined similarly for the nearby skeletal muscle, used as reference tissue. All the MR images were analyzed using ImageJ (https://imagej.nih.gov/ij/) to get the signal intensity and the area of each ROI. The calculated %NSE values are reported in Table S5.

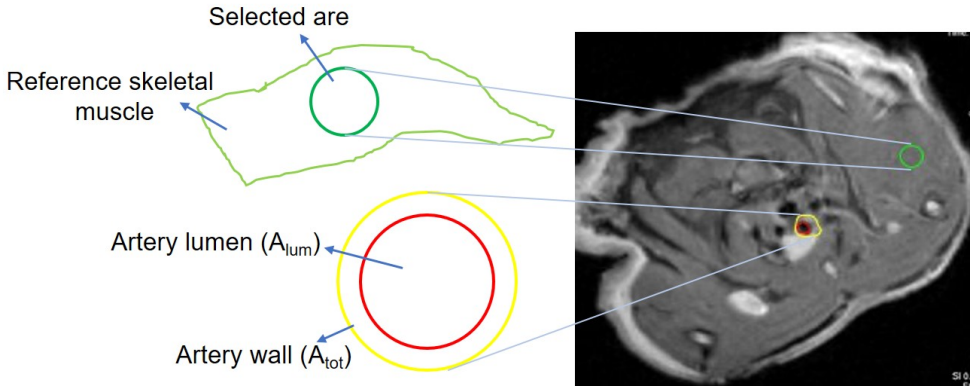

Figure S43. Example image for the determination of the %NSE. The yellow line delimits the external area of the artery wall (A_{tot}), the red line delimits the area of the artery lumen (A_{lum}), and the green line delimits the area of the skeletal muscle used as reference tissue.

[7] Yamaskoshi, Y.; Qiao, H.; Lowell, N. A.; Woods, M.; Paulose, B.; Nakao, Y.; Zhang, H.; Liu, T.; Lund-Katz, S.; Zhou, R. LDL-based nanoparticles for contrast enhanced MRI of atheroplaques in mouse models. *Chem. Commun.* **2011**, *47*, 8835-8837.